NOVA SCHOOL OF SCIENCE & TECHNOLOGY

DEPARTMENT OF PHYSICS

JOÃO CARLOS TOMÁS DA SILVA

Bachelor's Degree in Biomedical Engineering Sciences

MODELING THE INFLUENCE OF FORMALIN FIXATION TIME ON THE ELEMENTAL CONSTITUTION OF HUMAN TISSUES

MASTER IN BIOMEDICAL ENGINEERING

NOVA University Lisbon
September, 2022

NOVA SCHOOL OF SCIENCE & TECHNOLOGY

DEPARTMENT OF PHYSICS

MODELING THE INFLUENCE OF FORMALIN FIXATION TIME ON THE ELEMENTAL CONSTITUTION OF HUMAN TISSUES

JOÃO CARLOS TOMÁS DA SILVA

Bachelor's Degree in Biomedical Engineering Sciences

Advisers: Prof. Dr. Alda Sofia Pessanha de Sousa Moreno
Assistant Researcher, NOVA School of Science and Technology
Prof. Dr. Jorge Felizardo Dias Cunha Machado
Principal Researcher, NOVA School of Science and Technology

MASTER IN BIOMEDICAL ENGINEERING

NOVA University Lisbon
September, 2022

Modeling the influence of formalin fixation time on the elemental constitution of human tissues

To my Family.

Acknowledgements

This master thesis was one of the hardest, most givinful works I have ever done. It marks the end of an incredible journey and the beginning of a new exciting one. I will do my best to express gratitude to everyone that helped me in this work and in this 5 years.

Having just my name on the front cover is not fair, since I could have not accomplish it without the help of many people.

I will start by thanking to the people without whom this dissertation would not have been possible. To my advisors, for being an example to me, for their guidance, for everything they taught me and for helping me whenever I needed and for making me fall in love with this life. Thank you Professora Sofia Pessanha and thank you Professor Jorge Machado. I will also thank Professor João Cruz for all the help in CTN, Professor Ana Félix, Doctor Fernanda Silva, all the unit at IPO, Ana Ensina, Patrícia Carvalho, Alexandre Veiga, Daniel Braga and Ricardo Castelhano for allowing me to use their previous studies in this area.

Now, to my inner circle. First of all to my family, for always believing in me, for doing everything for me, this one is for you. Mãe, Pai, Mano, Avó, Avô and Pité, thank you from the bottom of my heart. I will try to make you guys proud.

To Henrique, Cleto and Moisés for being the best friends I could have ever asked for, never forgetting me and always being there for me even when their lives are chaotic.

To Matilde, a special thank you for being my partner in crime on this journey, for listening and never giving me up. For always believing in me, even when I could not. Thank you for the unconditional love.

Thank you to Redentouros for beginning and ending this life with me, you are my university family for life.

To Braga and Babel, for parenting me through this journey and for always supporting me.

"Nothing in life is to be feared, it is only to be understood."
(Marie Curie)

Abstract

Cancer is a leading cause of death worldwide, accounting for nearly 9.6 million deaths. Therefore, an early and accurate diagnosis is essential. Trace elements are essential and are linked with toxicity when they exist in abnormal quantities. Thus, understanding the mechanisms of assimilation/accumulation of trace elements may be indicative of the genesis or progression of certain diseases, such as carcinogenesis.

X-rays have been employed in the medical system since its discovery, particularly for diagnostics and treatments. Micro Energy Dispersive X-ray Fluorescence (μEDXRF) is used as a multielement analysis technique of trace elements, once it measures non-destructively actual tissue levels of elements in very small portion of tissue, and it was the chosen one for this Master Thesis. Previous studies show that the formalin fixation time influences the elemental composition present on the tissue, focusing on the drastic decrease of K and Cl after 48 hours. In order to have an accurate quantification of this elements, we need to study the influence of formalin fixation time on tissues.

In this work, 6 sets of muscle tissues, from Instituto Português de Oncologia (IPO), submitted to different fixation times in formalin were analyzed with the goal to parameterize the influence of formalin fixation time on the elemental constitution of human tissues, focusing on 9 trace elements - K, Zn, Cl, P, S, Cu, Fe, Mn and Ca. The quantitative analysis was done using Certified Reference Materials (CRMs) to build elemental calibration curves. All the data was treated in different ways, namely with ROOT software - removing background and identifying each elemental peaks - and with the Compton-to-Rayleigh Ratio correction, in order to minimize errors and improve accuracy. Statistical tests, Shapiro-Wilk was performed to test the normality of the distributions of each element and Kruskal-Wallis ANOVA to compare the tissues with different fixation times.

The results obtained, confirmed what it was expected, showing that the K and Cl concentrations dramatically decrease in the first 3 hours of formalin fixation time.

Keywords: Cancer, Muscle, μEDXRF, μXRF, Trace Elements, Calibration Curves, CRM, FFPE, FF, IPO

Resumo

O cancro é uma das principais causas de morte em todo o mundo, sendo responsável por quase 9,6 milhões de mortes. Portanto, um diagnóstico precoce e preciso é essencial. Os elementos traço são essenciais e estão ligados à toxicidade quando existem em quantidades anormais. Assim, a compreensão dos mecanismos de assimilação/acumulação de elementos traço pode ser um indicativo do aparecimento ou progressão de certas doenças, como a carcinogénese.

Os raios-X têm sido usados no sistema médico desde sua descoberta, principalmente para diagnósticos e tratamentos. A μEDXRF é utilizada como técnica de análise multielementar de elementos traço, uma vez que mede, de uma forma não destrutiva elementos numa porção muito pequena de tecido, e foi a técnica escolhida para esta Dissertação de Mestrado. Estudos anteriores mostram que o tempo de fixação em formol influencia a composição elementar presente no tecido, focando na diminuição drástica de K e Cl após 48 horas. Para uma quantificação precisa desses elementos, precisamos estudar a influência do tempo de fixação em formol nos tecidos.

Neste trabalho, 6 conjuntos de tecidos musculares, do IPO, submetidos a diferentes tempos de fixação em formol foram analisados com o objetivo de parametrizar a influência do tempo de fixação em formol na constituição elementar dos tecidos humanos, com foco em 9 elementos traço - K, Zn, Cl, P, S, Cu, Fe, Mn e Ca. A análise quantitativa foi feita utilizando CRMs para construir curvas de calibração elementares. Todos os dados foram tratados de diferentes formas, nomeadamente com software ROOT - removendo o fundo e identificando cada pico elementar - e com a correção Compton-to-Rayleigh Ratio, de forma a minimizar erros e melhorar a precisão. Foram usados testes estatísticos, nomeadamente o Shapiro-Wilk para testar a normalidade das distribuições de cada elemento e o Kruskal-Wallis ANOVA para comparar os tecidos com diferentes tempos de fixação. Os resultados confirmaram o esperado, mostrando que as concentrações de K e Cl dramaticamente nas primeiras 3 horas de fixação em formol.

Palavras-chave: Cancro, Músculo, μEDXRF, μXRF, Elementos Traço, Curvas Calibração, CRM, FFPE, FF, IPO

Contents

List of Figures xi

List of Tables xiii

Acronyms xv

1 Introduction 1
- 1.1 Context and Relevance . . . 1
- 1.2 Objectives . . . 2

2 Fundamental Concepts of XRF 4
- 2.1 Properties of X-Rays . . . 4
- 2.2 Interactions of X-Rays with matter . . . 5
  - 2.2.1 Absorption . . . 5
  - 2.2.2 Scattering . . . 5
  - 2.2.3 Diffraction . . . 7
  - 2.2.4 Reflection . . . 8
  - 2.2.5 Emission . . . 8
- 2.3 X-Ray Fluorescence Spectroscopy . . . 10
  - 2.3.1 XRF Spectrometers . . . 10
  - 2.3.2 X-Ray Spectra . . . 12
- 2.4 XRF Analysis . . . 13

3 State of the Art 16
- 3.1 Analysis of Human Tissues Using EDXRF and TXRF . . . 16
- 3.2 Trace element analysis by SRIXE, PIXE and PIGE . . . 17
- 3.3 Formalin-Fixed Paraffin-Embedded Tissues . . . 18

4 Influence of formalin on Tissue's Elemental Content - Part I 20
- 4.1 Methods . . . 20
- 4.2 Sample Description . . . 21

4.3 Results and Discussion . . . 22
4.4 Conclusions . . . 24

5 Influence of formalin on Tissue's Elemental Content - Part II **25**
5.1 Materials . . . 25
5.1.1 Tissue Samples . . . 25
5.1.2 Formalin and Formalin Retainer Filters . . . 26
5.1.3 M4 Tornado - Micro X Ray Fluorescence . . . 26
5.1.4 ROOT . . . 28
5.2 Methods . . . 29
5.2.1 Sample Treatment . . . 29
5.2.2 Data treatment . . . 29

6 Results and Discussion **42**
6.1 Influence of Formalin Fixation Time on the Elemental Concentration of Tissues . . . 42
6.1.1 Influence of Formalin Fixation Time on K Concentration . . . 43
6.1.2 Influence of Formalin Fixation Time on Cl Concentration . . . 45
6.1.3 Influence of Formalin Fixation Time on Zn Concentration . . . 46
6.1.4 Influence of Formalin Fixation Time on P Concentration . . . 49
6.1.5 Influence of Formalin Fixation Time on S Concentration . . . 49
6.1.6 Accuracy of the Results . . . 50

7 Conclusions **52**
7.1 Future Work . . . 53

Bibliography **54**

Appendices

Annexes

List of Figures

2.1 Representation of the electromagnetic spectrum. X-rays correspond to 0.01 to 10 nm [9]. . . . 4
2.2 Rayleigh Scattering. Adapted from [9]. . . . 6
2.3 Compton Scattering. Adapted from [9]. . . . 7
2.4 Bragg's Law [11] 8
2.5 Comparison of the Fluorescence and Auger emission yield as a function of the atomic numbers. . . . 10
2.6 Illustration of a typical EDXRF Setup [9] 11
2.7 Illustration of a typical WDXRF Setup [9] 12
2.8 XRF spectra of the certified reference material Bovine Liver 185R with a Rh target source and Al 12.5 filter. Opened with Root. . . . 12
2.9 Plot of the comparison of the relative radiation intensity of Fe in different materials as a function of the Fe weight fraction. [12] 13

3.1 K, Cl and P concentration in tissue over time 18

4.1 Methodology applied to analyse the formalin 22
4.2 Comparison of the elemental concentration of paper filter retainer before and after addition of 200 μL of fresh formalin 23
4.3 Comparison of the elemental concentration of paper filter retainer after addition of 200 μL of formalin with different fixation times. . . . 23
4.4 Elemental maps in different stages of the analysis method 24

5.1 IPO Sample in Formalin 25
5.2 M4 Tornado Laboratory Setup 26
5.3 Sketch of the interior channels of a monolithic poli-capilary optic. Adapted from [32]. . . . 27
5.4 ROOT Logo 28
5.5 Sample treatment and pellet manufacturing 29
5.6 X-ray fluorescence spectrum of CRM Bovine Liver 185R with background . 31

5.7 X-ray fluorescence spectrum of CRM Bovine Liver 185R after the background removal with the peaks identified 31
5.8 CRMs data treatment example for the K 33
5.9 Concentration in the CRM as a function of the I(Kα) / I(C/R) ratio 34
5.10 Spectra obtained with M4 Tornado software of the 334 fresh sample 38
5.11 X-ray fluorescence acquired spectrum after background removal for the fresh sample 332 38
5.12 331 Fresh sample data treatment and determination of the K concentration (in μg/g). 39
5.13 Determination of K concentration (in μg/g) for different periods of time . . 40
5.14 Data Treatment Synthesis 41

6.1 Plot of the variation of the K concentration [μg/g] in IPO tissues as a function of fixation time in formalin. 43
6.2 Shapiro-Wilk normality test for K 44
6.3 Kruskal-Wallis ANOVA test for K 44
6.4 Plot of the variation of the Cl concentration [μg/g] in IPO tissues as a function of fixation time in formalin. 45
6.5 Shapiro-Wilk normality test for Cl 46
6.6 Kruskal-Wallis ANOVA test for Cl 46
6.7 Plot of the variation of the Zn concentration [μg/g] in IPO tissues as a function of fixation time in formalin. 47
6.8 Shapiro-Wilk normality test for Zn 48
6.9 Kruskal-Wallis ANOVA test for Zn 48
6.10 Plot of the variation of the P concentration [μg/g] in IPO tissues as a function of fixation time in formalin. 49
6.11 Plot of the variation of the S concentration [μg/g] in IPO tissues as a function of fixation time in formalin. 50

List of Tables

4.1 Comparison of the elemental concentrations (μg/g) for Whatman paper obtained in this work and in and by Manso et al. [29] 22

5.1 Information about the IPO Samples Formalin Fixation Time 26
5.2 Excitations Specifications used on M4 Tornado 27
5.3 Measurement Conditions on M4 Tornado 28
5.4 Kα and Energy Kβ energies, in keV, of K, Ca, Mn and Fe 32
5.5 Comparison of the NIST certified P concentration and the obtained using the calibration curves for NIST SRM 1566b Oyster Tissue and NIST GBW 07605 Tea (in μg/g). 35
5.6 Comparison of the NIST certified S concentration and the obtained using the calibration curves for NIST SRM 1566b Oyster Tissue and NIST GBW 07605 Tea (in μg/g). 36
5.7 Comparison of the NIST certified Cl concentration and the obtained using the calibration curves for NIST SRM 1566b Oyster Tissue and NIST GBW 07605 Tea (in μg/g). 36
5.8 Comparison of the NIST certified K concentration and the obtained using the calibration curves for NIST SRM 1566b Oyster Tissue and NIST GBW 07605 Tea (in μg/g). 36
5.9 Comparison of the NIST certified Ca concentration and the obtained using the calibration curves for NIST SRM 1566b Oyster Tissue and NIST GBW 07605 Tea (in μg/g). 36
5.10 Comparison of the NIST certified Mn concentration and the obtained using the calibration curves for NIST SRM 1566b Oyster Tissue and NIST GBW 07605 Tea (in μg/g). 36
5.11 Comparison of the NIST certified Fe concentration and the obtained using the calibration curves for NIST SRM 1566b Oyster Tissue and NIST GBW 07605 Tea (in μg/g). 36

5.12 Comparison of the NIST certified Cu concentration and the obtained using the calibration curves for NIST SRM 1566b Oyster Tissue and NIST GBW 07605 Tea (in μg/g). 37
5.13 Comparison of the NIST certified Zn concentration and the obtained using the calibration curves for NIST SRM 1566b Oyster Tissue and NIST GBW 07605 Tea (in μg/g). 37

6.1 Comparing the obtained values of K concentration 50
6.2 Comparing the obtained values of Cl concentration 51

Acronyms

μEDXRF Micro Energy Dispersive X Ray Fluorescence 16, 17, 21
μXRF micro X Ray Fluorescence 2, 11, 26

CRM Certified Reference Materials xi, xii, 15, 17, 22, 28, 29, 30, 31, 32, 33, 34, 35, 37, 42

EDXRF Energy Dispersive X Ray Fluorescence xi, 2, 3, 11, 16, 20, 21
ESM External Standard Method 14, 15, 16, 17

FFPE Formalin-Fixed Paraffin-Embedded Tissues 2, 16, 18, 20, 52
FPM Fundamental Parameter Method 14, 16, 17

ICA Influenced Coefficient Algorithms 14
IPO Instituto Português de Oncologia xi, xiii, 25, 26
ISM Internal Standard Method 14

NIST National Institute of Standards and Technology xiii, xiv, 30, 32, 35, 36, 37, 42

PIGE Proton-Induced Gamma-ray Emission 17
PIXE Proton-Induced X-ray Emission 17

SAM Standard Addition Method 15
SRIXE Synchrotron Radiation Induced X-ray Emission 17

TXRF Total Reflection X Ray Fluorescence 11, 16, 17, 21

WDXRF Wavelength Dispersive X Ray Fluorescence xi, 11, 12
WHO World Health Organization 1

XRF X Ray Fluorescence ix, xi, 1, 2, 4, 7, 10, 12, 13, 16, 17, 18, 20, 32, 42

1

Introduction

This section contains the context and relevance of this work, the main goals aimed and a brief explanation of the fundamental concepts regarding this work's developments.

1.1 Context and Relevance

Major elements, minor elements and trace elements form the mineral constituents of biological tissues. Trace elements are essential and in very limited quantity in humans, usually acting as a specific activator of organic complexes and are linked with toxicity when they exist in abnormal quantities [1]. Thus, understanding the mechanisms of assimilation/accumulation of trace elements may be indicative of the genesis or progression of certain diseases, such as carcinogenesis.

According to the World Health Organization (WHO), cancer occurs when aberrant cells develop out of control, cross their normal borders to infiltrate surrounding body parts and/or move to other organs. The latter process is called metastasizing and is a major cause of death from this disease. Cancer is a leading cause of death worldwide, accounting for nearly 9.6 million deaths in 2018. Nonetheless, besides this large number of deaths and the estimated total annual economic cost of cancer (in 2010 was around 1.16 trillion US$), it is estimated that 30-50% of cancers could be prevented [2]. In order to reduce the number of people that suffer and die from cancer every year, it is important to see the early signs of carcinogenesis. Given this, many epidemiologic studies have been undertaken to identify potential risk factors for cancer, amongst which the association with trace elements has received considerable attention. [3].

X-rays have been employed in the medical system since its discovery, particularly for diagnostics and treatments. X-ray Fluorescence (XRF), Compton Effect, and X-ray Diffraction can provide details about the composition and structure of human tissues. Thus, the main objective of non-imaging X-ray techniques has been to distinguish tissues (cancerous, benign or healthy) [4], namely with the quantification of trace elements.

XRF is used as a multielement analysis technique of trace elements, once it measures non-destructively actual tissue levels of elements in very small portion of tissue [5, 6].

Through the years there have been many advances in XRF instrumentation: the development of cameras that produce pictures based on X-ray effects with excellent spectrum resolution; X-ray optics, such as polycapillaries, which are becoming more specialized and enable microfocusing with diameters as tiny as 10 µm. These developments allowed the appearance of high-resolution versions of the XRF technique such as μXRF.

The analysis of elemental composition in human tissues, in pathological anatomy or other diagnostic techniques, usually comprises a time of fixation and preservation in formalin. Altough the samples can be snap-frozen, Formalin-Fixed Paraffin-Embedded (FFPE) tissue specimens have been a staple of research and therapeutic applications for a long time, since snap-freezing has some disadvantages, such as inconvenient storage and handling. Formalin is a simple but important member of aldehydes, is highly reactive due to its strong electrophilic properties. It is a substance frequently used in medicine to preserve human tissues or cells, through the formalin fixation process, as mentioned previously, which is the first step in the process of paraffin inclusion to human tissue conservation and it fixes tissues or cells by cross-linking the proteins. Formalin is widely used as fixative due to its low cost, simplicity of use and good fixation traits, which are fast tissue penetration, good preservation of morphological structures and compatibility with downstream histological applications.

Previous studies show that the formalin fixation time influences the elemental composition present on the tissue [7], focusing on the drastic decrease of K and Cl after 48 hours. The effect of freezing the samples has been considered innocuous [8], however, the influence of time in formalin on the elemental composition of tissues is not studied or parameterized and this is needed in order to take advantage of the large repository of FFPE samples existing in Hospitals throughout the country. The effect caused by variations in the quantity of trace elements, after three days of formalin fixation time will be covered in this work.

1.2 Objectives

The main goal of this work is to develop a parameterization model of elemental concentration as a function of time preserved in formalin.

In order for that goal to be accomplished, three more goals must be fulfilled first. Those are:

- Controlled formalin incubation of the snap-freezing tissue samples over different periods of time, followed by sample preparation for Energy Dispersive X-ray Fluorescence (EDXRF) analysis in order to gauge variations in the concentration of some trace elements.

- Development of a methodology for analyzing liquid samples with EDXRF, in order to study the changes in the elemental composition of formalin. This development is

important because if the concentration of the elements in the tissue decreases after the formalin fixation, they might have migrated somewhere, probably the formalin;

- Acquisition, deconvolution and quantification of EDXRF spectra;

2

Fundamental Concepts of XRF

This section contains the theoretical concepts behind this work.

2.1 Properties of X-Rays

X-rays have wavelengths and energies between the low energy gamma rays' range and the high energy ultraviolet range, as shown on the figure 2.1,

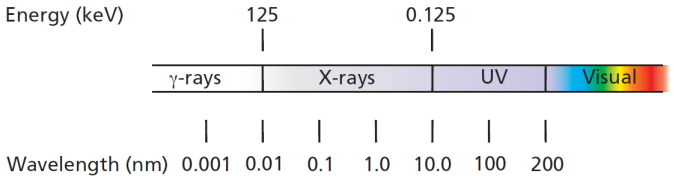

Figure 2.1: Representation of the electromagnetic spectrum. X-rays correspond to 0.01 to 10 nm [9].

The wavelengths of X-rays are in the range from 0.01 to 10 nm, which corresponds to energies in the range from 0.125 to 125 keV. The wavelength of X-rays is inversely proportional to its energy given by the equation 2.1:

$$E = h \times \frac{c}{\lambda} \tag{2.1}$$

where E is the energy (in keV), h is the Planck's constant (4.14×10^{-15} eVs), c is the speed of light (3.00×10^{8} m/s) and λ is the wavelength (in nm). [10].

X-rays are produced by deceleration of high-energy electrons and by electrons transitions in the inner orbital of atoms. They propagate in straight lines, are invisible and are undetectable by other human sense. When striking matter, X-rays may be transmitted, reflected, diffracted, scattered, or undergo photoelectric absorption. Interactions with matter result in production and emission of photoelectrons, auger electrons, spectral lines, and continuum radiation. The core of X Ray Fluorescence (XRF) Spectrometry is based on the last two mentioned properties and only a small portion of x-ray spectrum is used in XRF spectrometry

2.2 Interactions of X-Rays with matter

It is necessary to have a basic grasp of the interactions between the incident X-rays and the samples in order to interpret the acquired X Ray Fluorescence spectra. Due to the small wavelengths of this radiation, which are in the range of atomic distances in solid and liquid material, as well as its strong penetration, provide a variety of options for material analysis [11].

Absorption, scattering or diffraction, refraction, and emission are some of the X-ray interactions with materials that can be exploited.

2.2.1 Absorption

When X-ray beam impinges on a material, characterized by an atomic number Z, they interact with it and will be attenuated. This interaction is described by the mass absorption coefficient, μ, which is given by [11]:

$$\mu = \tau + \sigma \tag{2.2}$$

where τ (in cm^2/g) and σ (in cm^2/g) represent the absorption and scattering, respectively.

Lambert-Beer's law can be used to explain attenuation. So, the mass attenuation coefficient μ, the material density ρ, and the thickness of the material t, all influence absorption. This implies that the incident radiation's intensity will be reduced:

$$I(\lambda_0) = I_0(\lambda_0)\exp(-\mu \cdot \rho \cdot t) \tag{2.3}$$

where $I(\lambda_0)$ is the primary intensity, μ (in cm^2/g) is the mass attenuation coefficient as function of energy, ρ (in g/cm) is the density of the absorbing material and t (in cm) is the thickness of the absorbing layer. The mass attenuation coefficient in equation 2.3, depends on the energy of the radiation, therefore it depends on the radiation wavelength, λ_0.

If the material is composed of distinct elements, the mass attenuation coefficient can be calculated multiplying all of the mass attenuation coefficients for all of the elements contained in the specimen by each mass fraction w_i [11]:

$$\mu_{compound} = \sum w_i \mu_i \tag{2.4}$$

where w_i is the mass fraction of element i and μ_i is the mass absorption coefficient of element i.

2.2.2 Scattering

In these phenomena, Rayleigh and Compton Scattering, there is a deflection of the X-ray photon upon colliding with the electron of an atom. This scattering can be described by the classical electromagnetic theory, meaning Rayleigh Scattering, as well as with

the particle model for X-ray photon, meaning Compton Scattering. The scattered X-rays behave differently in both descriptions [11].

2.2.2.1 Rayleigh Scattering:

Rayleigh scattering is described by the electromagnetic theory which describes an elastic scattering, in which the scattered X-ray loses no energy. It is also known as coherent scattering.

In this scattering process, the scattered photon has the same energy as the incident photon, because the electron absorbs the energy of the incident photon and transits to a virtual state as a result. When it returns to its original condition, it emits the scattered photon, which has the same energy as the incident photon but travels in a different direction, as shown in figure 2.2.

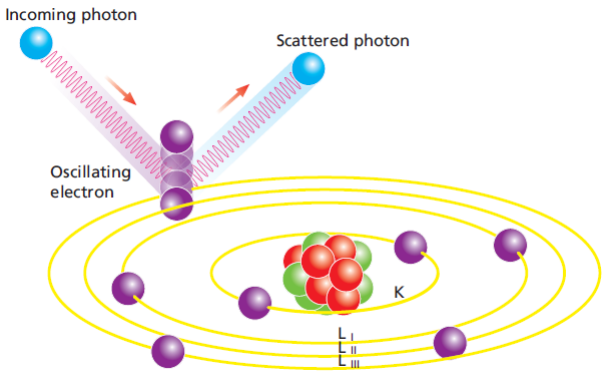

Figure 2.2: Rayleigh Scattering. Adapted from [9].

The atom is neither ionized nor excited in this process. For randomly distributed directions of the electromagnetic field of X-rays, the Rayleigh scattering is given by [11]:

$$I_{scat} = I_0 \frac{1}{r^2} \left(\frac{e^2}{m_0 c^2} \right)^2 \cdot \left(1 + \cos^2 \varphi\right) \tag{2.5}$$

where I_{scat} is the scattered intensity, I_0 is the primary intensity, r is the distance to the observation point, e is the charge of an electron (1.602×10^{-19} coulombs) , m_0 is the mass of an electron, c is the speed of light (3.00×10^8 m/s) and φ is the scatter angle.

According to this formula, there is no change in energy, however there is a dependence on the scatter angle. The scattered intensities are high for angles φ close to 0 or 180. On the other hand, they are minimum for scattering with angles close to 90, i.e., scattering perpendicular to the incident beam.

2.2.2.2 Compton Scattering:

Compton scattering is described by the corpuscular nature of X-ray photon. So, when the X-ray photon hits an electron, energy and momentum are transferred from the photon to

the electron, as shown in figure 2.3.

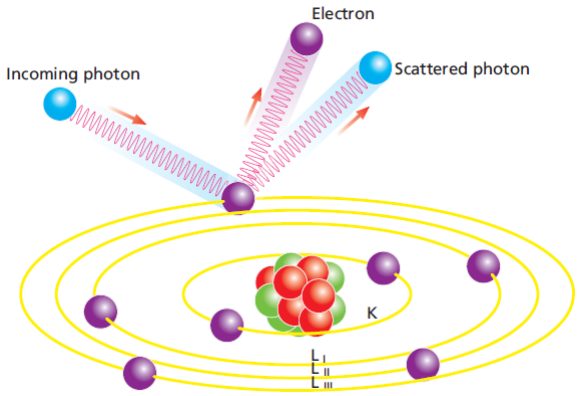

Figure 2.3: Compton Scattering. Adapted from [9].

Therefore, both energy and momentum conservation are valid for the process and the energy loss of the photon depends on its scatter angle. Compton scattering is also known as incoherent or inelastic scattering since the scattered photon has lost energy. The wavelength of the photon increases as a result of the energy loss [11] and is described by:

$$\lambda_{scat} = \lambda_0 + \lambda_c \cdot (1 - \cos\varphi) \tag{2.6}$$

where λ_{scat} (in nm) is the wavelength of the scattered radiation, m is the mass of the scattering particle (considered an electron in this case), λ_0 (in nm) is the wavelength of the incident photon, φ is the scatter angle and λ_c (in nm) is the Compton wavelength given as follows:

$$\lambda_c = \frac{h}{mc} \tag{2.7}$$

where m is the mass of the scattering particle (electron in this case).

At high energy incoming photons and low Z elements, Compton scattering is preferred, whereas Rayleigh scattering is preferred at low energy incident photons and high Z elements.

Even though these two interactions do not cause fluorescence, they can cause peaks in the XRF spectrum, which might be valuable for quantitative study.

2.2.3 Diffraction

Diffraction is the result of a mixture of coherent scattering and interference (the effect of one wave superimposed on another). Only when the difference in path-lengths of the

two interfering waves is equal to a full number of wavelengths can the reinforcement condition for reflection (also known as Bragg's law) occur:

$$n \cdot \lambda = 2d \cdot \varphi \tag{2.8}$$

where λ is the wavelength of the scattered radiation, d is the spacing of the scattering lattice and φ is the scatter angle.

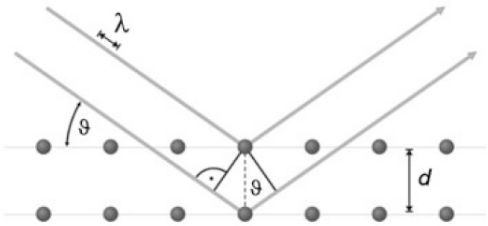

Figure 2.4: Bragg's Law [11]

2.2.4 Reflection

When X-rays pass through areas with different optical densities, they are refracted. The density of the material has a big impact on X-ray refraction. That is, the higher the density, the less refractive the material is. The X-ray refraction is described by:

$$n = 1 - \delta + i\,\beta \tag{2.9}$$

where β is the absorption coefficient and δ is a possible derivation.

2.2.5 Emission

This subsection describes the two types of X-ray emission: Characteristic Radiation and Continuous Radiation.

2.2.5.1 Emission of Characteristic Radiation:

The absorption of X-rays in matter, mentioned on the subsection 2.2.1, can either amplify lattice oscillations or excite atoms by the emission of a photoelectron, designated as Photoelectric Effect (PE). This electron might even arise from the atom's inner shells due to the high energy of the incoming X-ray.

If outside electrons fill the vacancy in this shell, the atom enters the ground state, allowing energy to be radiated as electromagnetic radiation. The energy of this radiation is normally in the X-ray range. This process is known as X-ray fluorescence because it may be triggered by radiation, or emission of characteristic radiation, meaning its energies are characteristic to the atom involved. So, in X-ray fluorescence, when sample atoms are irradiated with high-energy primary X-ray photons, electrons are ejected in the form of

photoelectrons. This creates electron "holes"in one or more of the orbitals, converting the atoms into ions - which are unstable. To restore the atoms to a more stable state, the holes in inner orbitals are filled by electrons from outer orbitals. Such transitions may be accompanied by an energy emission in the form of a secondary X-ray photon. The various electron orbitals are called K, L, M, etc, where K is the closest to the nucleus. Each corresponds to a different energy level. The mass attenuation coefficient μ, described on the subsection 2.2.1, determines the intensity of emitted radiation. That means, the energy of these emitted photons depends on the element and on the energy difference between the two involved shells in the transition of the electron. As a result, the emitted characteristic radiation is unique for each element, allowing for accurate identification of those components in a sample. However, this simply refers to the occurrence of a vacancy in an inner electron shell. This void must be filled by an outside electron, which varies depending on the transition. The energy difference between the binding energy of the two electron shells of this transition:

$$E_{diff} = E_{vacancy} - E_{outer} \tag{2.10}$$

can be emitted directly by an X-ray which is the characteristic radiation [11].

The other possibility is the emission of an Auger-electron. In Auger electron emission, the filling of the hole in the inner shell is made by an electron from one of the outer shells and is accompanied by the ejection of an electron from the outer shell. In this case, the excess of energy in the atom, after removing one electron, does not result in the emission of X-ray photons but in the ejection of an electron from the outer shell. As the atom is left in a doubly ionized state, because two electrons are missing, the energy associated to the electron that is leaving is given by:

$$E_{Auger} = E_{diff} - E_{binding} \tag{2.11}$$

The probability of the Auger effect becomes higher when the difference between the corresponding energy states decreases [11]. Because there is only one possible method for energy emission, the probability of their aggregate must be unit:

$$p_{Auger} - p_{X-ray} = 1 \tag{2.12}$$

Fluorescence yield, ω, is the probability of an X-ray emission, and it is dependent on energy and the electron transition [11]. Auger electron emission is preferred for low-atomic-number atoms, whereas X-ray florescence takes over for high-atomic-number elements as it can be observed in figure 2.5:

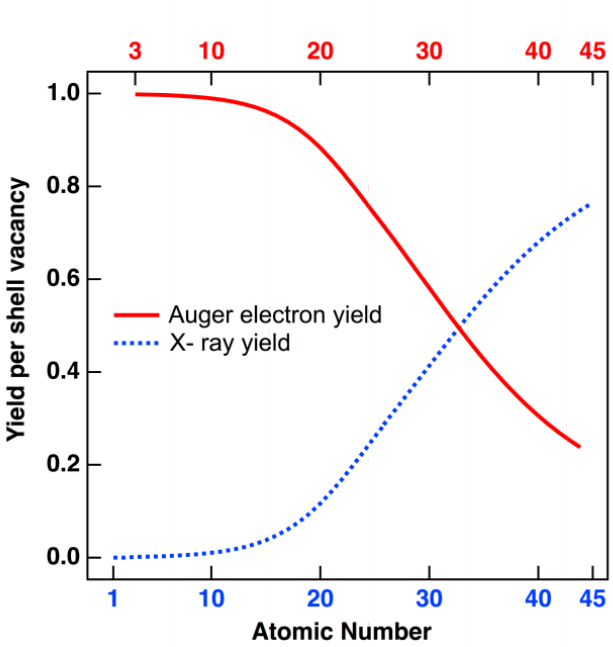

Figure 2.5: Comparison of the Fluorescence and Auger emission yield as a function of the atomic numbers.

2.2.5.2 Emission of Continuous Radiation:

Alternatively, to the characteristic radiation, with discrete energies, in the energy range of X-rays, there is also continuous radiation, named Bremsstrahlung Radiation. According to basic electromagnetic theory, high-energy charged particles can be decelerated when they pass through the coulomb field of an atom nucleus, resulting in the emission of a broad wavelength band of radiation known as Bremsstrahlung Radiation [11].

2.3 X-Ray Fluorescence Spectroscopy

2.3.1 XRF Spectrometers

As mentioned in the subsection 2.2, when striking matter, X-rays may be transmitted, reflected, diffracted, scattered, or undergo photoelectric absorption. Their interaction with matter can result in the production and emission of photoelectrons, Auger electrons, spectral lines, and continuum radiation. The core of XRF Spectrometry is based these properties.

Even though the X-ray region on the electromagnetic spectrum overlaps with the low energy gamma rays' range and the high energy ultraviolet range, only a small portion of the X-ray spectrum range is used for XRF spectrometry.

X Ray Fluorescence Spectroscopy techniques allow the element quantification in a non-destructive manner, which means it does not damage the sample. The main concept

for all spectrometers is a source which irradiates a sample. There is also a detector that measures the radiation from the sample. There are two possible spectrometers setups:

- Energy Dispersive X-ray Fluorescence (EDXRF) – Uses a detector that can sort the energies of the photons, as shown in the figure 2.6. It can measure all elements simultaneously and the area of the peak profile determines the concentration of the element. It uses a special x-ray detector that gives the distribution of voltage pulses proportional to the energy of the electron photons. In EDXRF systems, different types of X-ray sources can be used, the most common are synchrotron radiation sources, radioactive sources and X-ray tubes. In this work, a system with an X-ray tube was used, a suitable option for laboratory use, easy handling and affordable, with applicability in the analysis of biological tissues. It has the advantages of being low-cost and making fast measurement times. However, the energy resolution due to broad overlapping peaks is a disadvantage. The EDXRF setup is also not very suitable for light elements. Total Reflection X-ray Fluorescence (TXRF) and micro X-ray Fluorescence (μXRF) are two variations that come from EDXRF. While in TXRF the angle between the X-ray tube and the sample is almost identical to the total reflection angle of X-rays in a reflector Si wafer, allowing that only the photons emitted by fluorescence phenomena are detected, in μXRF the X Rays are focused to a much smaller area, improving the spatial resolution.

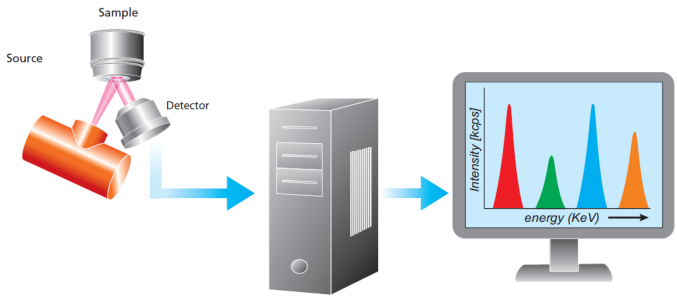

Figure 2.6: Illustration of a typical EDXRF Setup [9]

- Wavelength Dispersive X Ray Fluorescence (WDXRF) Uses a crystal to select which wavelength radiation enters the detector, as shown in the figure 2.7. In that crystal, the x-rays are scattered from different layers of atoms, which means that some beams travel a longer optical path. As an advantage, it presents greater accuracy, than the EDXRF setup. It is well suited for lighter or heavier elements. However, it has some disadvantages, such as longer measurement times and significantly higher cost of the spectrometer.

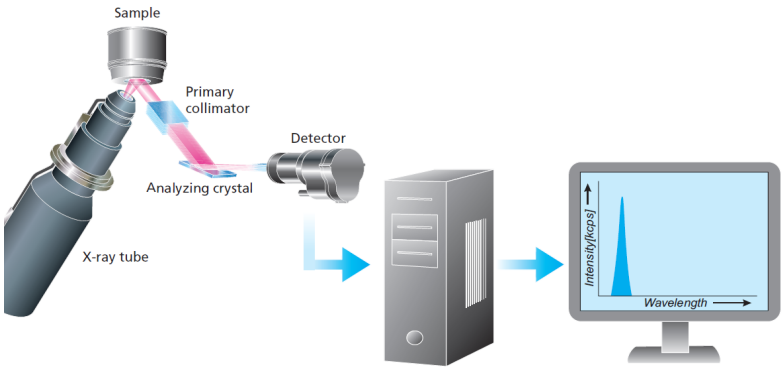

Figure 2.7: Illustration of a typical WDXRF Setup [9]

2.3.2 X-Ray Spectra

A X-ray spectra includes two main features, a well-defined continuum, and sharp characteristic lines, as shown in the figure 2.8.

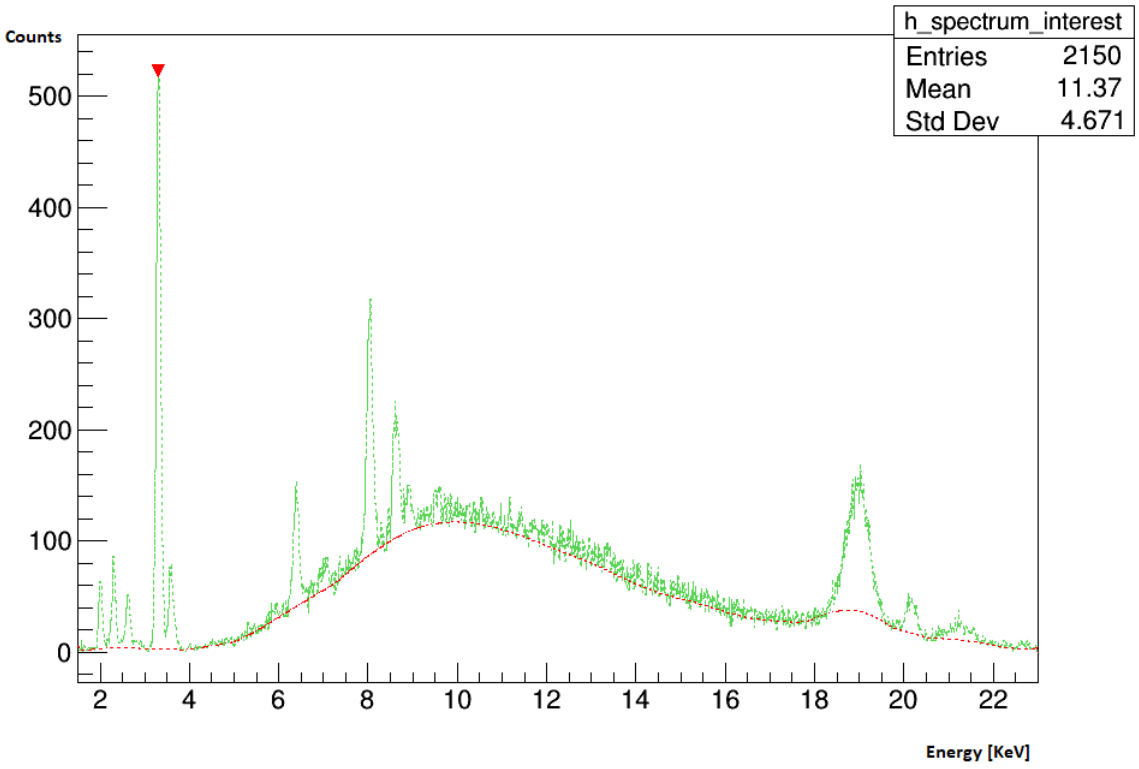

Figure 2.8: XRF spectra of the certified reference material Bovine Liver 185R with a Rh target source and Al 12.5 filter. Opened with Root.

The interaction of each photon in this Bremsthalung radiation through Compton and Rayleigh is referred to as the spectrum background. The intensity of the energy scatter produced by Bremsstrahlung radiation is inversely proportional to the atomic number of

the element from which the electron came. However, there is a way to reduce background in the measurement, using filters. Filters are placed between the source and the sample. They reduce the intensity of interfering lines and background, improving the signal-to-noise ratio [9].

2.4 XRF Analysis

X-ray Fluorescence is mostly a direct analysis i.e., without dilution, and therefore the matrix is strongly changing with every sample, enhancing matrix interaction. When quantifying elements in a sample, matrix effects can attenuate or enhance fluorescence photons due to their interaction with matrix elements, affecting the peaks' intensity in the XRF spectrum.

The strong matrix interaction of XRF causes that an approach of the measured intensities to the corresponding weight fractions is not possible for a wide range of weight fractions with linear calibration curves. Furthermore, because the matrix interaction has altered, new calibrations are necessary for different qualitative compositions. That is, the measured element intensities are impacted by all other elements in the sample as well as the measurement conditions and the element weight fraction itself [9].

The absorption and enhancement effects can be seen in figure 2.9 using samples of binary composition, where Fe has the same concentration in all compounds. This comparison shows how the relative intensity of the peaks in a XRF spectrum corresponding to an element (in this case Fe) can be influenced by the presence of other elements in the sample.

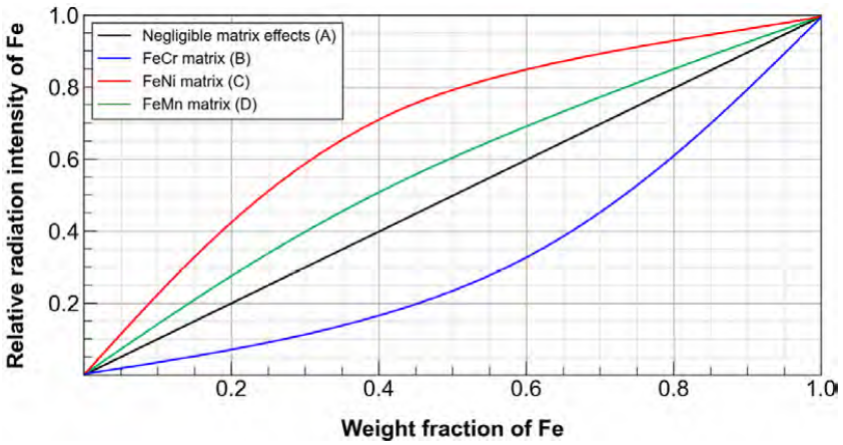

Figure 2.9: Plot of the comparison of the relative radiation intensity of Fe in different materials as a function of the Fe weight fraction. [12]

When matrix effects are either negligible or constant, it is obtained the curve A which is a linear relation between radiation intensity and weight fraction of analyte. In Curve B the absorption by the matrix elements in the specimen is stronger than the absorption by

the analyte alone. Because Fe's characteristic energy is greater than Cr's binding energy, Cr can be ionized by this energy, resulting in a drop in intensity as indicated in curve B. In this scenario, the intensity of the peaks will suggest that there is less Fe in the sample than there actually is. In Curve C occurs the opposite, illustrating an enhancement effect. Fe has a lower binding energy than the characteristic energy of Ni, resulting in the ionization of Fe due to Ni. Meaning that the intensity of the peaks would imply that the sample has more Fe than it does. Curve D is observed when the matrix element in the specimen absorbs the analyte radiation to a lesser degree than the analyte alone. The characteristic energies of the elements are very similar, so the ionization of the elements is less probable to happen, resulting in a curve close to A [12].

Matrix effects are negligible for thin samples, as a result, the peak intensity is proportional to the concentration of these elements.

Due to the problems that the matrix effects can bring, there are two groups of methods that can either correct or compensate them: Matrix Correction Methods and Compensation Methods. One of the advantages of the Matrix Correction Methods is that it does not require any sample preparation. Whichever method chosen, all the interactions on X-ray analytics can be described by physical models [11].

There are two Matrix Correction Methods:

- Fundamental Parameter Method (FPM) – Iterations are used to determine the composition of a given sample. The theoretical intensities are compared to the experimental intensities of the assumed composition, assuming a particular composition for the study sample. Then, the composition is adjusted until the theoretical and experimental spectrums match up [12]. However, this method can be difficult to use in human tissues, where the sample matrix contains elements that are not visible in the XRF spectrum but have a significant impact on how trace elements are detected, such as H, C, N, and O.

- Influenced Coefficient Algorithms (ICA) – Based on obtaining numerical coefficients, that correct the influence of matrix effects on the intensity of the detected radiation, through mathematical formulas, using regressions.

On the other hand, there are three Compensation Methods:

- Internal Standard Method (ISM) – Consists of introducing a known quantity of an element not present in the sample, but with similar fluorescence properties, to the sample. The peak intensity corresponding to that element will be used as a standard for quantifying the other components in the sample. This method is appropriate for thin samples, as while the sample thickness increases, linearity is lost, and matrix elements must be considered.

- External Standard Method (ESM) – As mentioned on ISM, when the thickness increases, matrix elements must be considered. So, an effective method to overcome

this issue is ESM. Consists of quantifying the components of a given sample by comparing them to Certified Reference Materials (CRM) of similar composition than the unknown, without any mixing. It is vital to admit that the matrix remains constant during the comparison in this procedure.

- Standard Addition Method (SAM) – Requires introducing the element under interest into the sample at defined concentrations and examining the former and resultant effects of this introduction. It is not well suited for studying elements in low concentrations due to the need of preparing the sample and the difficulty in obtaining known concentrations.

3

State of the Art

This section contains the state of the art of the quantification and identification of trace elements in human tissues using XRF, the effect of formalin in FFPE tissues and liquid sample analysis techniques with EDXRF.

3.1 Analysis of Human Tissues Using EDXRF and TXRF

X-ray Fluorescence techniques have been widely used for the detection and quantification of elements in a sample.TXRF and EDXRF are the most widely utilized XRF methods for detecting trace elements in human tissue. In a study performed by Magalhães *et al.*, he considered both techniques to be complementary, concluding that EDXRF is more suitable for heavier elements and TXRF is more sensitive to lighter elements [13].

Approximately 99% of the weight of the average human body is mainly composed of four elements - H, O, C and N - and the remaining is made up of minor - Na, K, Mg, Ca, Cl, P, S - and trace - Mn, Fe, Cu, Zn, Se - elements [14]. This trace elements, due to their physiochemical properties can cause oxidative DNA damage or trigger the stimulation of malignant growth. Carcinogenic stress can be exposed by inadequate concentrations or lack of trace elements [1].

In [15] and [16], TXRF was used to found statistically different the concentrations of P, S, K, Ca, Fe, Ni, Se, and Rb in healthy and cancerous tissues in several tissue samples. An increase in concentrations of breast malignant neoplasm tissues was observed, as compared to breast benign neoplasm tissues. Magalhães *et al.* performed a study using both EDXRF and TXRF, checking an increase of most of the trace elements (mainly Fe, Cu and Zn) including Br in breast carcinoma [13].

In a study performed by Ensina *et al.*, it was used μEDXRF as a tool, due to being a non-destructive technique, to characterize the tissues. In this research two different methods of quantification were compared - Fundamental Parameters Method (FPM) and the External Standard Method ESM - after the determination of the dark matrix. One of the conclusion drawn was that the FPM approach rendered much more precise results, as the uncertainty is much lower than the ESM approach. Probably, due to other analyte

elements' influence in the quantification, that is taken into calculation by the FPM approach, while using a calibration curve (ESM), does not consider matrix effects. Some discrepancies also occur in some samples for the lighter elements - P, S and K - that were expected since the matrix effects are more important and affect lighter elements due to self-absorption effects [14].

Machado *et al*. [17] applied the external standard calibration approach in the quantitative determination of elemental concentration in human , using the μEDXRF system M4 Tornado - Bruker. In this study, several calibration curves with the combination of two sets of CRMs, one set of animal tissues CRMs and other set with plant leaves CRMs, were constructed, aiming to improve the accuracy of quantitative determinations of elements present in human tissues by XRF spectrometry. This improved approach was tested on five paired samples of normal and tumour human tissue and all data was analysed using the advanced spectra processing tools of ROOT [18]. Reference samples were shown to be more accurate when used collectively than when used separately and despite the high heterogeneity of the samples, significant differences in the elemental concentration of low-Z elements, like K, were discovered. However, for some well-known trace elements like Fe and Zn there was not seen any significant variations. The described methodology above will be used in my thesis.

3.2 Trace element analysis by SRIXE, PIXE and PIGE

Breast tumor tissue is one of the pathological tissues that has been investigated the most regarding its elemental composition. Techniques including TXRF, Synchrotron Radiation Induced X-ray Emission (SRIXE), and Particle Induced X-ray Emission (PIXE). All of these techniques detected increased levels of trace elements like, bromium, zinc, iron, copper and others [19], [20], [21]. In [22], Gherase *et al*. stated that synchrotron-based in vitro studies of various human tissues showed significant differences between the normal and pathological distributions of metallic trace elements such as iron, zinc, copper, and lead in relation to human diseases ranging from Parkinson's disease and cancer to osteoporosis and osteoarthritis. Particle Induced Gamma-ray Emission (PIGE) is also an highly multi-element used technique, since it is possible to establish several relations between light elements present in tissue samples, like sodium. In a study performed by K. Nomita Devi *et al*., PIXE and PIGE techniques were employed for the determination of essential and trace elements, as they complement each other. Light elements such as Na, Mg, Al and P are determined by PIGE while medium Z elements such as K, Ca, Mn, Fe, Cu, Zn, Rb and Sr are determined by PIXE [23].

3.3 Formalin-Fixed Paraffin-Embedded Tissues

FFPE is one of the most used fixation techniques in medicine. In a study, Paunesku et al. [24], stated that previous studies have determined that FFPE preserve their morphology very well and can be used for the quantification of elements.

However, Joanna Chwiej *et al*. determined the concentration of Br, Ca, Cu, Cl, Fe, K, P, Rb, S, Sr, and Zn for fixed tissues and paraffin-embedded tissues with standard reference materials. On the obtained results there was an increase in the concentration of Cu, Fe, P, S, and Zn and a decrease for Br and K due to fixation in formalin before embedding in paraffin to be examined and a decrease in concentration for almost all elements due to paraffin [7].

In recent studies, the obtained results show that formalin influences XRF measurements. It was possible to see an alteration in concentration after just 2 days of fixation time for the lighter elements - S, K, Cl and P. The decrease in Cl and K was around 90%, after the second day [25]. Conversely, no significant changes were observed for Zn, Cu, S, and Ca.

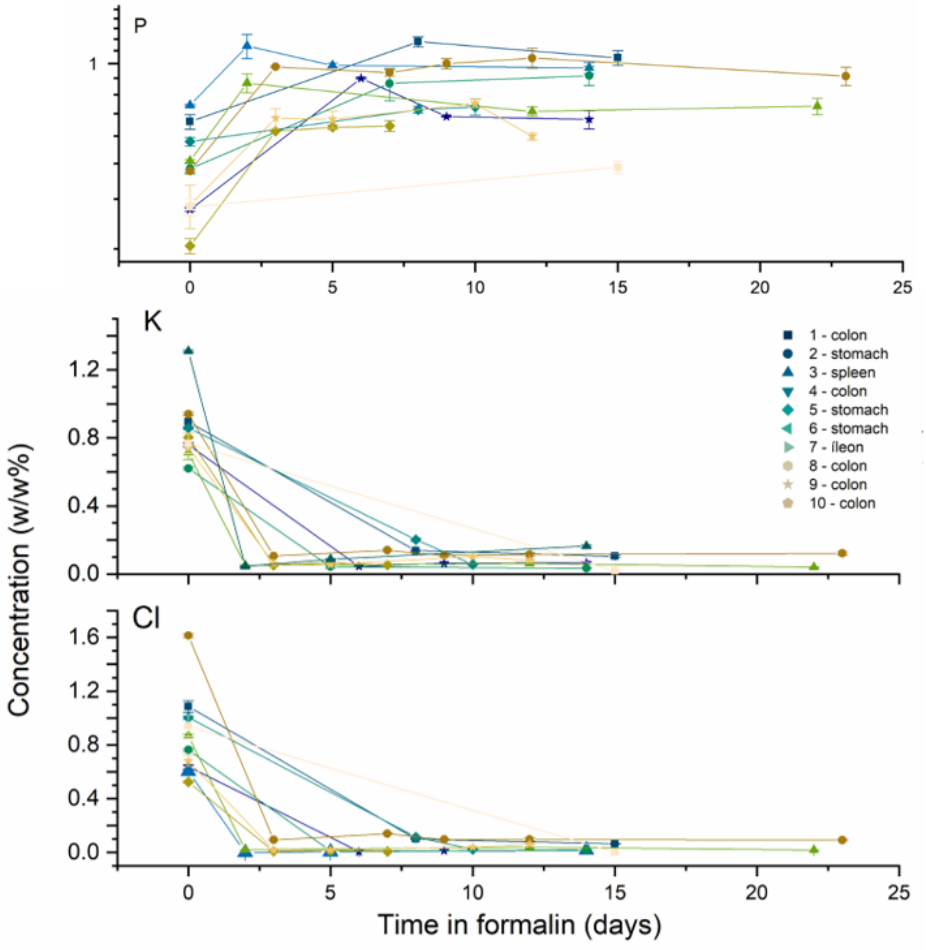

Figure 3.1: K, Cl and P concentration in tissue over time

Consequently it is of extreme importance to understand where did Cl, K and Ca migrate to. If their concentration was decreased on the tissue, one possibility is that the elements stayed in the formalin. Thus it is important to analyse the liquid samples of formalin.

4

Influence of formalin on Tissue's Elemental Content - Part I

Previous works, which gave rise to my thesis, proved that the concentration of some trace elements varied after a tissue sample was subjected to formalin [25], [26]. However, formalin was never measured to verify if there was an increase or decrease in the concentration of these trace elements. This section - Part I - has a brief explanation of what was done with the formalin, in which old tissue samples were fixated (from 2 to 24 days), namely its quantification to legitimize the work I proposed.

4.1 Methods

The most widely used method for tissue preservation and fixation during transportation between hospital departments is the conservation in formalin during variable amounts of time. Moreover, if there is a need to study Formalin-Fixed Paraffin Embedded (FFPE) tissue blocks stored in medical centres, which is the case of this master thesis project, one must account for the formalin fixation period of the tissues before embedding. Although the information regarding the impact of the formalin fixation time and the elemental concentrations is scarce, as mentioned on the section 3.3, previous studies have reported variations of the mass per unit area of some elements [25], [7].

XRF techniques are usually employed for the analysis of solid samples, since liquid samples present high X-ray scatter background, poor signal-to-noise ratio and high uncertainty results. To overcome the challenge of analysing complex liquid samples with EDXRF, Pessanha et al. studied multielemental analysis of mining water samples with a sustainable and reliable triaxial pXRF method - 3pXRF. In this method many microliters of sample were deposited onto a commercial filter paper retainer and after drying, the loaded filter is directly analyzed in the field using a laboratory pXRF with orthogonal triaxial geometry (3pXRF). This geometry reduces the background of the measured spectra improving peak-background ratios in comparison with conventional pXRF systems [27].

The results obtained presented an acceptable accuracy and precision in comparison

with laboratory techniques such as inductively coupled plasma optical emission spectrometry and total reflection X-ray fluorescence spectrometry TXRF [27]. The potential of 3pXRF method was corroborated for multielemental analysis of mining water samples, but its application could be extended for liquid sample studies.

Compared to other atomic spectrometry techniques, EDXRF constitutes the ideal compromise of non-invasiveness, simple instrumentation, and good sensitivity. For these reasons, this technique has already been tested in the quantitative analysis of human tissues. Then the chosen technique for this work was the μEDXRF setup M4 Tornado, described later in chapter 5, choosing the methodology used in the 3pXRF study [27], described above.

Consequently, to understand the influence of formalin fixation time in the elemental composition of human tissue samples, ten sets of human tissue samples (from the colon, ileum, stomach, and spleen) were exposed to various formalin fixation times ranging from 2 to 24 days, and the formalin solution was subjected to EDXRF analysis in order to further assess element translocation.

4.2 Sample Description

Samples (cold ischemia < 10 min) were collected from 10 surgical specimens and divided into cubes with approximately 1 cm^3. One portion of each set was snap-frozen, and the remaining portions were preserved in a 10 % v/v formalin buffered solution (4% formaldehyde stabilised with methanol 0.5-1.5 %, VMR Chemicals, USA) until removal from the vials, according to different time-frames, between 2 and 24 days and studied in previous works [25].

In order to study the transference of elements to-from the formalin solution where the sets of human tissue samples were exposed [A], 200 μL of formalin from each container were pipetted to paper filter retainers, microcarry (Rigaku, Japan), following the methodology developed for the analysis of liquids samples using μEDXRF [27]. Lastly, the paper filter retainers with formalin undergo an μEDXRF analysis with the M4 Tornado [C], as shown in 4.1. To ensure that the edge effect was taken into account, and surpass that issue, 21 × 21 mm^2 area acquisitions were performed with the measurement conditions and excitation parameters of the M4 Tornado specified in 5.1.3, yielding an acquisition time of, approximately, 40 minutes. The procedure was repeated with a sample of fresh formalin in order to know its concentration.

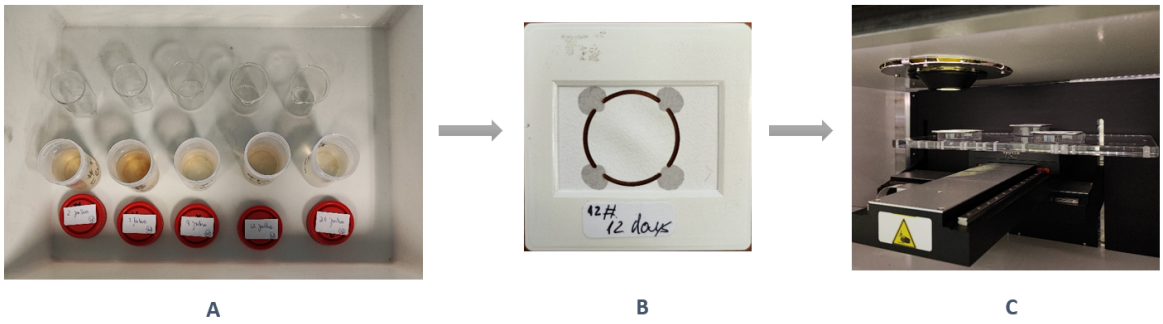

Figure 4.1: Methodology applied to analyse the formalin

Quantification of the paper retainer filters was performed with empirical calibration curves, using the following leaves Certified Reference Materials (CRM), whose matrix is cellulose: bush branches and leaves GBW 07603, poplar leaves GBW 07604, orchard leaves NBS1571, and tea leaves GBW 07605). This procedure has been previously applied to ancient documents by Manso et al. [28]. The method's accuracy was assessed using a sample of Whatman paper for conservation purposes, of known concentration [29], and the results are present in table 4.1.

Table 4.1: Comparison of the elemental concentrations (μg/g) for Whatman paper obtained in this work and in and by Manso et al. [29]

	Reference value, [29]	Obtained value
S	1300 ± 170	1400 ± 200
Cl	750 ± 90	700 ± 30
K	50 ± 12	77 ± 7
Ca	1000 ± 40	1300 ± 200
Fe	20 ± 2	17 ± 3
Cu	5 ± 1	5 ± 1
Zn	5 ± 1	4 ± 1

4.3 Results and Discussion

Following the presented results by [25], described in 3.3, and to evaluate the migration of elements between formalin and tissue, the solutions in which each tissue was fixated were analyzed. Figure 4.2 shows the comparison of the elemental concentration of the filter retainer before and after the addition of 200 μL of fresh formalin. As can be seen, P concentration increases (6000 ± 300 μg/g) after the addition of fresh formalin, when compared to the sterile paper filter. This could be due to the use of buffered formalin, important to stabilize the pH in the solution, typically using sodium phosphate. Regarding K and Cl, no alteration was verified.

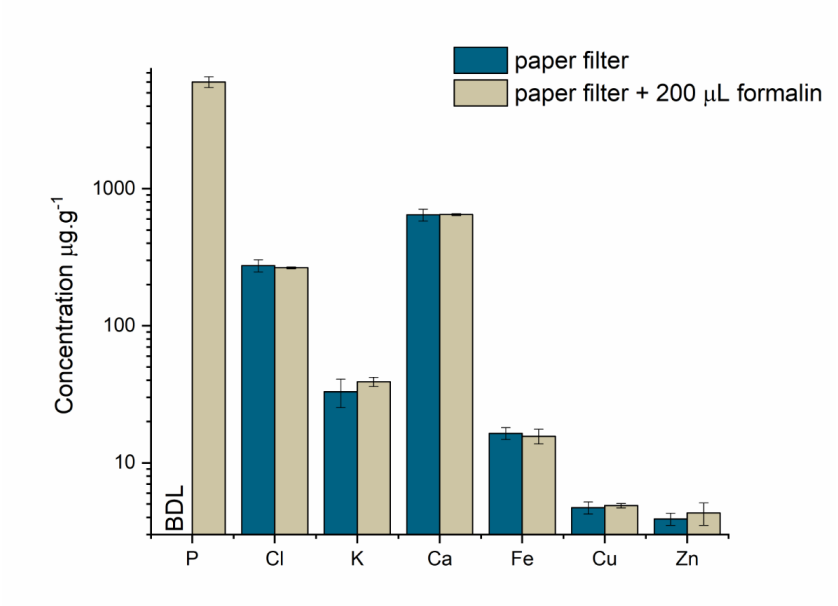

Figure 4.2: Comparison of the elemental concentration of paper filter retainer before and after addition of 200 μL of fresh formalin

Finally, using sample set #7 as the example for the longest time in formalin (24 days), figure 4.3 shows the variation of elemental concentration of paper filter deposited with formalin for different fixation times, compared to fresh formalin.

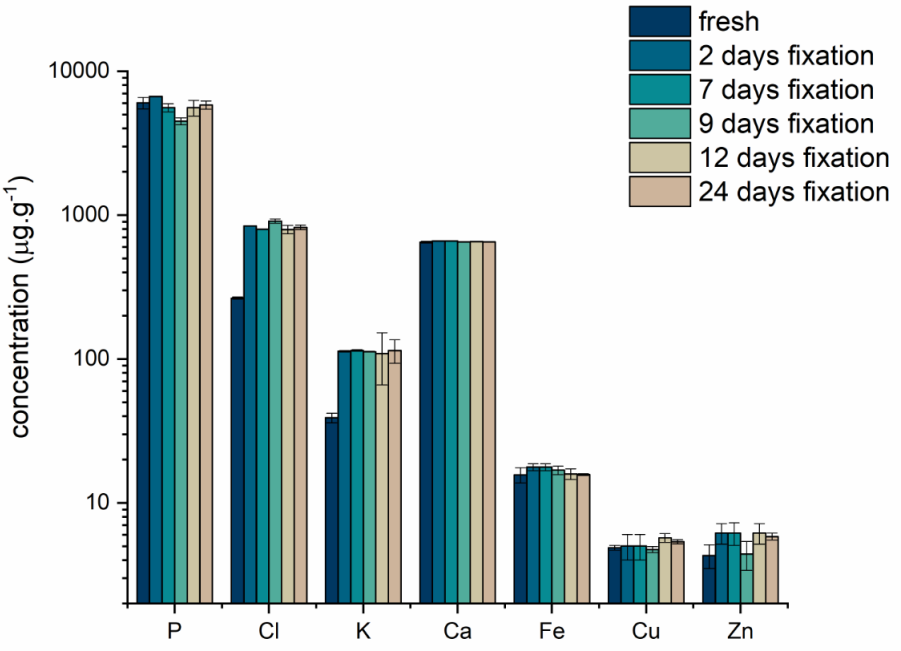

Figure 4.3: Comparison of the elemental concentration of paper filter retainer after addition of 200 μL of formalin with different fixation times.

As can be seen, there is a clear increase of Cl and K after tissue fixation, while the variation of the concentration of elements such as Fe, Cu, and Zn is not considerable and

could be a consequence of inhomogeneity of the paper filter. Regarding P, although a decrease could be expected, due to incorporation in the tissue, it was not observed likely because of the high-volume ratio formalin/tissue.

These results corroborate the obtained elemental maps that are shown in figure 4.4. As can be seen, there is no considerable signal for K, Cl and P in the paper filter, the signal for P increases after addition of fresh formalin and after fixation, the signal for Cl and K also show a remarkable increase.

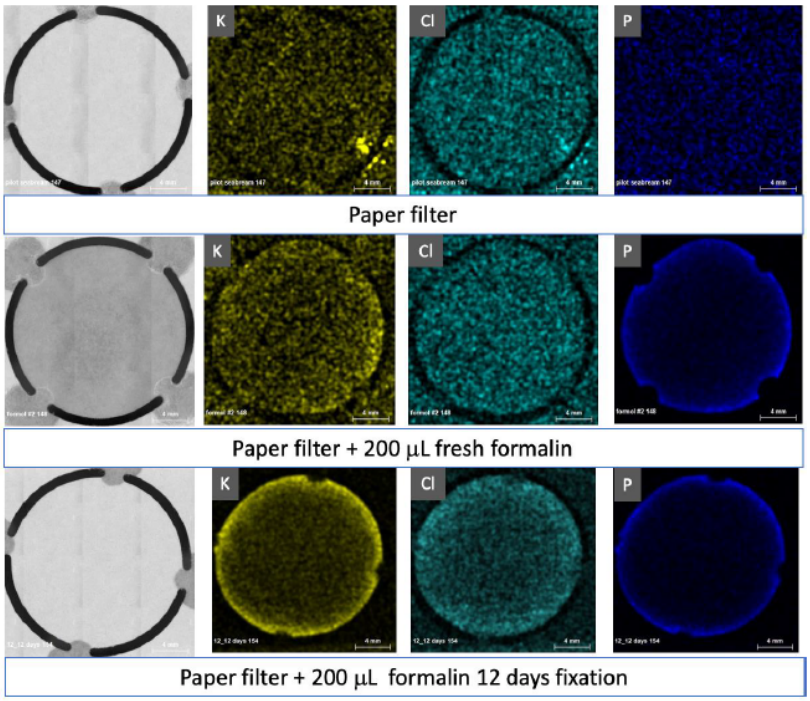

Figure 4.4: Elemental maps in different stages of the analysis method

4.4 Conclusions

Regarding the results obtained in this preliminary phase, it is verified the need to study the influence that time has on the elemental tissues concentration. It was determined the alterations induced by formalin in the elemental composition of tissues after fixation during different periods of time and how this should be taken into account when analysing tissues that have been stored in formalin or preserved as Formalin Fixed Paraffin Embedded blocks. The influence of formalin fixation time in the elemental composition of human tissue samples was evaluated and the results showed a clear decrease of Cl and K in the tissues, transferred to the formalin solution, on the first 48 hours. Conversely, there is a P uptake from the P present in formalin, likely due to the buffering solution. Given this, in this master thesis it will be studied the elemental exchanges occurred before 48 hours of fixation, so that thresholds for the influence of formalin fixation in human tissue can be established.

5

Influence of formalin on Tissue's Elemental Content - Part II

After analysing the formalin, in which old tissue samples were fixated from 2 to 24 days it was verified the need to study the elemental exchanges occurred before that time. This section - Part II - has a an explanation of what was done, in order to study the influence of formalin in the first 48 hours of fixation. Contains a deeper description of the materials used in this work as well as the methodologies applied to reach the objectives.

5.1 Materials

5.1.1 Tissue Samples

The samples were provided by the IPO - Instituto Português de Oncologia de Lisboa Francisco Gentil-, thanks to Professor Ana Félix and Doctor Fernanda Silva, and were transported to the laboratory in a freezing state, in order to preserve the elemental constitution. In the laboratory tissue samples were fixated in formalin in controlled time and then lyophilized. Only normal tissue was selected for this research, hence, the amount of obtainable tissue was scarce. The samples consist of surgically removed muscle tissue from individuals during biopsies.

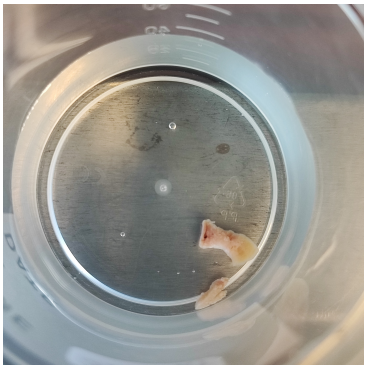

Figure 5.1: IPO Sample in Formalin

IPO samples are 6 sets of muscle tissue - 328, 329, 330, 331, 332 and 334. There was an attemp to padronize the sample size and formalin volume, however, due to the scarcity of removed normal tissue during biopsies, not all tissue samples had the required 1 cm^3. Also, for sample set 328, only 8 samples were obtained. Table 5.1 shows the sets and their sample distribution by time in formalin.

Table 5.1: Information about the IPO Samples Formalin Fixation Time

Set of samples	**Time in Formalin (hours)**								
	0	0.25	0.5	1	3	4.5	6	24	48
328	x		x	x	x	x	x	x	x
329	x	x	x	x	x	x	x	x	x
330	x	x	x	x	x	x	x	x	x
331	x	x	x	x	x	x	x	x	x
332	x	x	x	x	x	x	x	x	x
334	x	x	x	x	x	x	x	x	x

5.1.2 Formalin and Formalin Retainer Filters

It was used a 10 % v/v formalin buffered solution (4% formaldehyde stabilised with methanol 0.5-1.5 %, VMR Chemicals, USA), provided by IPO, with the aim of evaluate the transference of elements to and from the formalin solution. Each sample was fixated in 30 cm^3 of fresh formalin at the controlled times shown in table 5.1. Subsequently, 200 μL of formalin, from each container, were pipetted to paper filter retainers, microcarry (Rigaku, Japan), as decribed in Chapter 4.

5.1.3 M4 Tornado - Micro X Ray Fluorescence

Micro X-ray Fluorescence (μXRF) is an elementary non-destructive analysis technique that allows analysis at locations with a diameter of less than hundreds of micrometers [30] with good sensitivity for the elements of interest (Al=13 < Z < 83=Bi) of this study. This technique employs a direct X-ray excitation to cause a sample's characteristic radiation emission [11]. In this present work it was used the (μXRF) system M4 Tornado, from Bruker [31], as shown in the figure 5.2.

Figure 5.2: M4 Tornado Laboratory Setup

This system allows the analysis of the elements present in a material, being possible to perform a spot analysis, as well as mappings that cover an area chosen by the user (used in this thesis to analyse the formalin and the tissue pellets). In order to control the system and all its components the software MQuant was used.

Through it, it is possible to choose the area to analyse, what filter to use, the time of the measurement, the positioning of the sample, the parameters of the X-ray tube, and much more. The M4 Tornado allows to excellent spatial resolution using polycapillary X-ray optics for smallest spot sizes < 25 μm for Mo-K, 5 filters and vacuum sample chamber for optimized light element performance [31] and it is equipped with video cameras for real-time image transmission and correct positioning of the sample.

Poly-capillary optics are arrays of hollow glass tubes with diameters less than 2 μm used to collect, focus, and redirect x-ray and neutron beams [32]. A typical poly-capillary fiber is shown in figure 5.3. Poly-capillary optics increases the sensitivity of the technique in the analysis of trace elements.

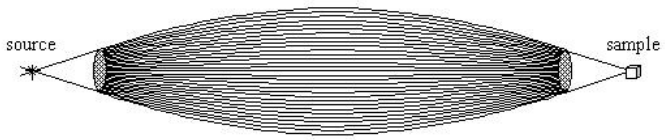

Figure 5.3: Sketch of the interior channels of a monolithic poli-capilary optic. Adapted from [32].

The acceleration of high voltage electrons against a metal target (anode) in an X-ray tube produces the X-ray beam that impinges on the sample. The target used is an Rh target. The X-ray beam travels via a poly-capillary lens after leaving the source and through multiple total reflections focus the beam on an area of 25 μm.

The excitation specifications used in this study on M4 Tornado are shown in table 5.2:

Table 5.2: Excitations Specifications used on M4 Tornado

Excitation Parameters	
Target	Rh
Filter	Al 12.5 with μm of thickness
Tube Parameters	50 kV, 300 μA
Spot Size	Less than 25 for Mo-K μm

In general, by lowering Bremsstrahlung radiation, the usage of filters enable an improvement in the peak-to-background ratio. In this instance, we are looking at substances that emit X-rays between 2 and 22 keV. To lessen the impact of the incident X-ray spectrum, filters must be used. In this master thesis project, the chosen filter was Al 12.5. Due to the high mass absorption coefficient for the mentioned energies, the Al 12.5 filter not only enables the removal of the L lines from the Rh X-ray tube employed in this study, but also improves the sensitivity of our detection. In order to acquire the spectrum of light elements, it is successfully applied.

5.1.3.1 Measurement Conditions

All the analyzes of this work were performed with the M4 Tornado. The M4 Tornado offers mapping and point-to-point analysis as its two acquisition modes. The mapping method was used because it enables the creation of a two-dimensional map of the distribution of the sample's constituents using equally spaced scanning lines. The measurement conditions are shown in table 5.3:

Table 5.3: Measurement Conditions on M4 Tornado

Measurement Conditions	
Formalin Filters Analytical Area	21 x 21 mm^2
Tissue Pellets and CRM Analytical Area	1 x 1 mm^2
Step	35 μm
Acquisition Time	4 ms/pixel

In order to avoid the presence of Argon in the measurements and also improve the sensitivity of our detection, all the analysis was done in vacuum conditions (approximately 20mbar).

5.1.4 ROOT

From the early stages of planning this work, it was clear that there would be the need for correcting the intensity of the characteristic peaks, removing the spectra background and increase the accuracy of the method. ROOT is an object-oriented program and library developed by CERN [33]. For this approach, the spectra were analyzed using the advanced spectra processing tools of ROOT [34].

Figure 5.4: ROOT Logo

All peaks present in the spectra were identified and the background estimated using the method based on the Sensitive Nonlinear Iterative Peak (SNIP) clipping algorithm [35]. A fit function composed of a sum of gaussian functions was then fitted to the spectra by X^2 minimization techniques. The number of peaks that were found, i.e., namely, the distinctive X-ray fluorescence peaks of each element present in the sample and the dispersion peaks, corresponds to the number of gaussians in the fit function. [17].

5.2 Methods

5.2.1 Sample Treatment

As mentioned before, the samples were transported to the laboratory in a freezing state and each sample was fixated in 30 cm^3 of formalin in controlled time. In figure 5.5 are displayed the various steps of the pellets manufacturing. After the time fixation in formalin, all the samples were lyophilized [A], so that all water content was removed from the sample [B], and powdered using a pestle and mortar in order to obtain a powder as much homogeneous as possible [C]. The obtained powder was pressed into pellets [D], positioned upon a Mylar film and placed on a slide frame [E]. Each tissue cube rendered only one pellet.

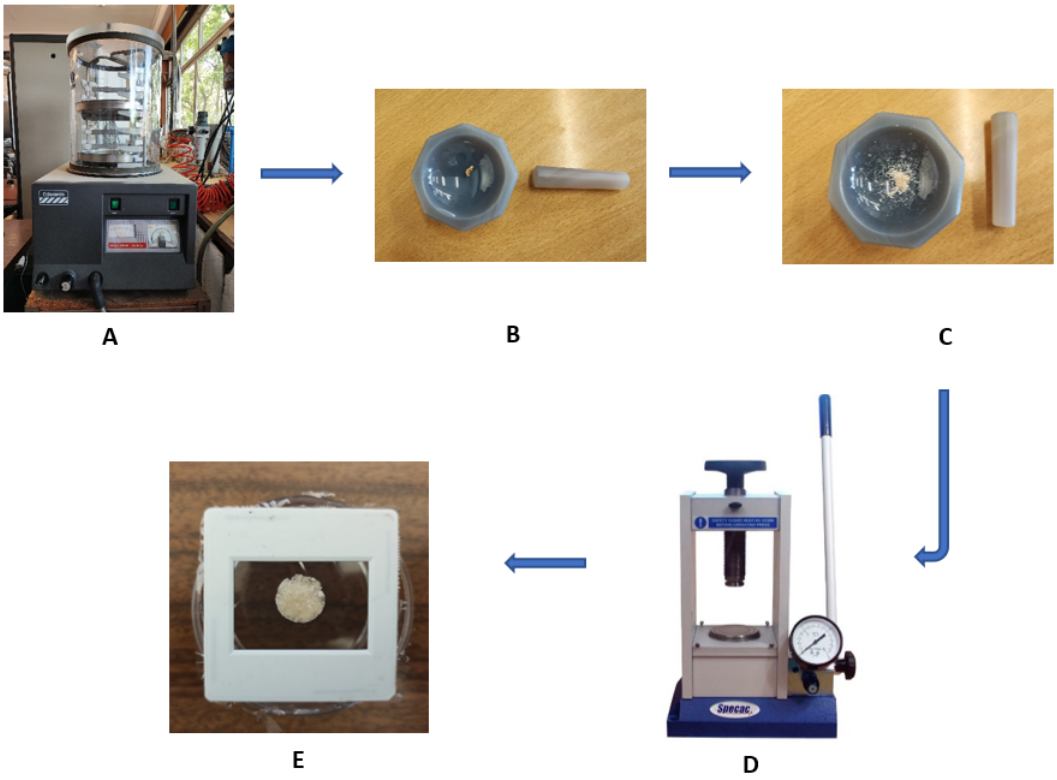

Figure 5.5: Sample treatment and pellet manufacturing

5.2.2 Data treatment

For this task, since it embraced a huge amount of data, the methodology was performed using Excel, ROOT and OriginLab. This subsection describes the entire process, since obtaining the spectra, until reaching the functions that describe the time influence of formalin in Ca, Cl, Cu, Fe, K, Mn, P, S and Zn concentrations. It starts by analysing CRM, with all the softwares mentioned above, in order to build elemental calibration curves for the external standard method of quantification, using the methodology described in [17]. Having reached a function that describes the elemental concentration and the Kα divided

by the Compton-to-Rayleigh ratio, validation was made with certified reference materials NIST SRM 1566b Oyster Tissue and NIST GBW 07605 Tea. Then, with a function for each interest element, tissue data was treated, reaching the elemental concentration from the Kα divided by the Compton-to-Rayleigh ratio obtained with the M4 Tornado. Applying it to all the tissues and respective times fixated in formalin, it was possible to reach the relation between time in formalin and elemental concentration proposed in the objectives of this master thesis and draw conclusions.

5.2.2.1 CRMs Background Removal and Peaks Finding

Three spectra were obtained from various regions of the sample and used to reduce statistical and surpass the issue of the heterogeneity of the pellets, ensuring that the analysis was as representative as possible of the average composition of the samples. This fact means that the final spectrum data will correspond to the average of the three spectra's values. As previously described, in order to build calibration curves for the external standard method of quantification, 12 animal and plant CRMs were used: NIST NBS 1577 Bovine Liver, NIST SRM 1566 Oyster Tissue, IAEA MA-A-2 Fish Flesh Homogenate, NRC-CNRC TORT-2 Lobster Hepatopancreas Reference Material for Trace Metals, ERM-BB186 Pig Kidney, BCR-185R Bovine Liver, DORM-2 Fish Protein certified reference material for trace metals,IAEA-359 Cabbage, NIST SRM 1571 Orchard Leaves, GBW 07603 Trace Elements in Bush Branches and Leaves, GBW 07604 Poplar Leaves, NIST SRM 1575 Pine Needles [36]. Additionally, further 2 CRMs, NIST SRM 1566b Oyster Tissue and NIST GBW 07605 Tea, were used in order to validate the curves.

After the acquisition of the sample's spectra, M4 Tornado exports 3 types of files, .txt, .bcf and .spx. Since the obtained spectrum is characterized by background radiation that is not needed to quantificate each sample, because by contributing to the apparent peaks it can give incorrect results, .txt file was used as an input to ROOT, not only to remove the background radiation, but also to identify the peaks, using the Sensitive Nonlinear Iterative Peak (SNIP) clipping algorithm, mentioned in 5.1.4. With no information available about the peaks other than their amount, the SNIP technique seeks to estimate the baseline of a spectrum by taking into account the linear and nonlinear portions of the peaks. For each sample, the variable containing the number of estimated peaks was changed on the script of the algorithm before running it in ROOT, once each sample could contain different elements. The energy range was set to a maximum value of 21 keV, since this was my elements range of interest.

Figure 5.6 shows the full X-ray fluorescence spectrum of CRM Bovine Liver 185R illustrated by the green line. The red dashed line represents the background estimation using the algorithm described above.

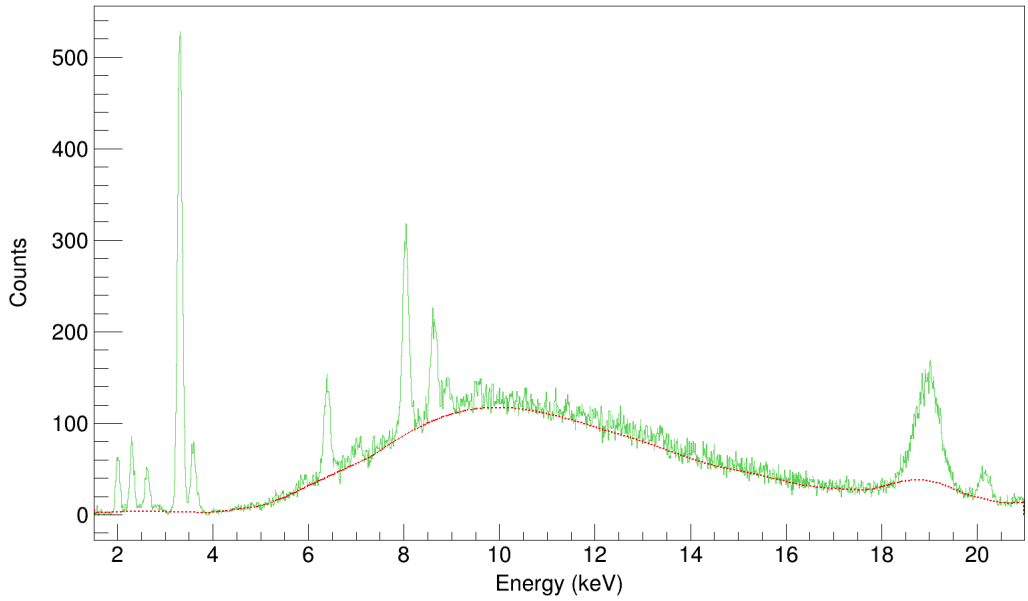

Figure 5.6: X-ray fluorescence spectrum of CRM Bovine Liver 185R with background

A Gaussian distribution is what defines an X-ray spectra peak. The location of the spectrum's peaks and their approximate conversion to Gaussian functions are the next steps after eliminating the background.

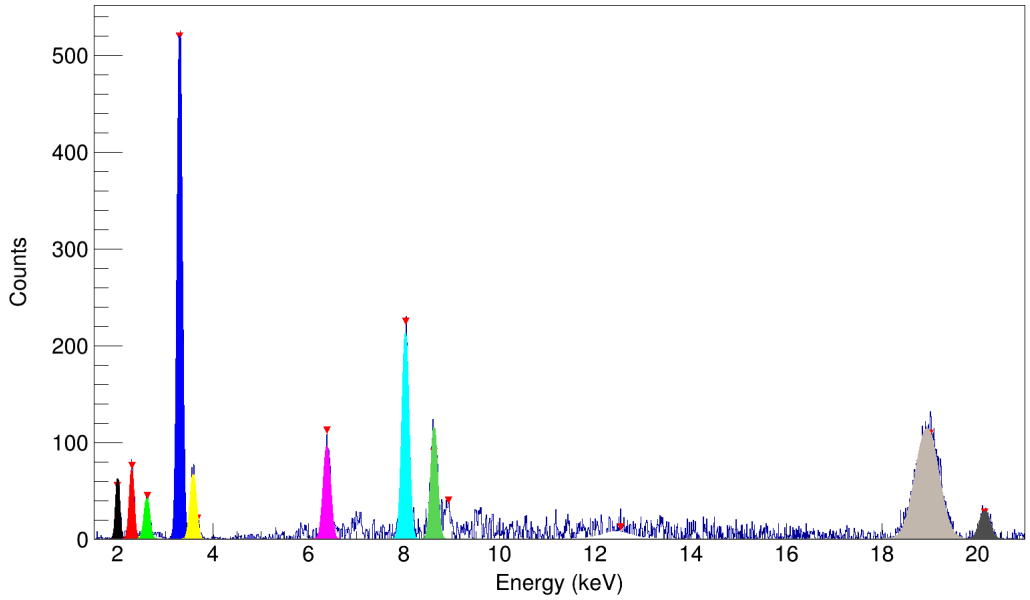

Figure 5.7: X-ray fluorescence spectrum of CRM Bovine Liver 185R after the background removal with the peaks identified

The algorithm uses a fit function composed of a sum of Gaussian functions and fits it to the spectra. The number of Gaussians of the fit function correspond to the number of the found peaks, i.e., the characteristic X-ray fluorescence peaks of each element present in the sample, and the dispersion peaks [17]. After identifying the characteristic peaks, the algorithm calculates the integrals associated with each peak and outputs not only the final treated spectra, as shown in figure 5.7, but also a peaksfits.txt file with the peak number, energy mean value, its uncertainty and the respective amplitude, which corresponds to the integrals associated with each peak.

In a XRF spectrum, the positions of the peaks, i.e., their characteristic energy value, determines the element. So, in order to identify which elements correspond to each energy value printed in peaksfits.txt, the NIST X-ray Transition Energies Database was consulted [37], linking the energy and Kα amplitude values to each element.

5.2.2.2 Peaks Correction and Compton-to-Rayleigh Ratio

Some interest elements' Kα and Kβ energies are not far from each other, i.e., the Calcium Kα and the Potassium Kβ energies are very close values, such as the Iron Kα and the Manganese Kβ energies, as shown in table 5.4. Thus, in order to reduce errors, avoiding that the Kα amplitude of Ca was not contributed the Kβ amplitude of K, each Kα amplitude of Ca was subtracted by each Kβ amplitude of K. The same process was applied to the Mn and Fe case. Starting from the relative intensities of K-shell X-ray emission rates (assuming Kα = 100) and the respective Kβ intensity, listed on [38], then was calculated which percentage of the amplitude value of Kβ corresponded to Kα, for K and Mn and subtracted to the Kα amplitude obtained values of Ca and Fe.

Table 5.4: Kα and Energy Kβ energies, in keV, of K, Ca, Mn and Fe

	Kα Energy	Kβ Energy
Potassium	3.312	3.589
Calcium	3.690	4.012
Manganese	5.894	6.489
Iron	6.398	7.057

As mentioned on the previous subsection, three spectrum were taken from different areas of the samples in order to reduce heterogeneity and have a deviation associated with our values, for each CRM. So, the values of the peaks' integrals of the average spectrum are the average of the integrals of the 3 spectra so that we have an error associated with our values. In order to reduce even more the errors and discard fluctuations, the normalization of Kα intensities by Compton-to-Rayleigh ratio was used in all of the samples before calculating the mean value for each sample. The Compton-to-Rayleigh ratio can be calculated by dividing the amplitude of the Compton and Rayleigh peaks corespondent to the characteristic radiation from the X-Ray source of the spectrometer, in this case Rh.

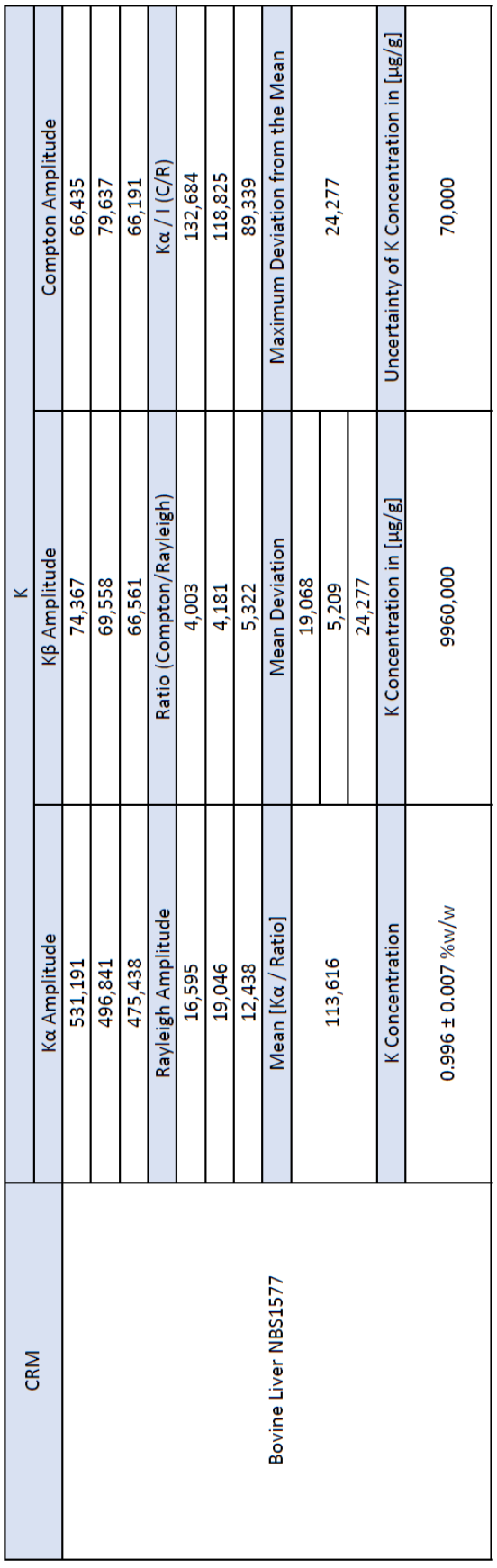

CRM	K								
	Kα Amplitude	Kβ Amplitude	Compton Amplitude						
	531,191	74,367	66,435						
	496,841	69,558	79,637						
	475,438	66,561	66,191						
	Rayleigh Amplitude	Ratio (Compton/Rayleigh)	Kα / I (C/R)						
	16,595	4,003	132,684						
	19,046	4,181	118,825						
	12,438	5,322	89,339						
	Mean [Kα / Ratio]	Mean Deviation	Maximum Deviation from the Mean						
	113,616	19,068	24,277						
		5,209							
		24,277							
	K Concentration	K Concentration in [µg/g]	Uncertainty of K Concentration in [µg/g]						
Bovine Liver NBS1577	0.996 ± 0.007 %w/w	9960,000	70,000						

Figure 5.8: CRMs data treatment example for the K

After determining the mean value for each CRM, the error used was the maximum deviation from the mean. For this, the differences between the values were calculated and the highest absolute value of these differences was considered. Since CRM concentrations, and the respective uncertainty, are known and well established, the next step is building the calibration curves for each element. Table 5.8 shows an example, for one of the interest elements for this master thesis, K, of complete Excel data treatment using one CRM, before using OriginPro to build the calibration curves. All the CRMs were submitted to the same analysis and concatenate in one table for each element.

5.2.2.3 Elemental Calibration Curves

After all the corrections and analysis, having all the needed data, the next step was the construction of the calibration curves for each given element through the Kα/Ratio and element concentration values and respectives deviations and uncertainties. Figure 5.9, shows the plot for the linear variation of K concentration, as a function of Kα/Ratio.

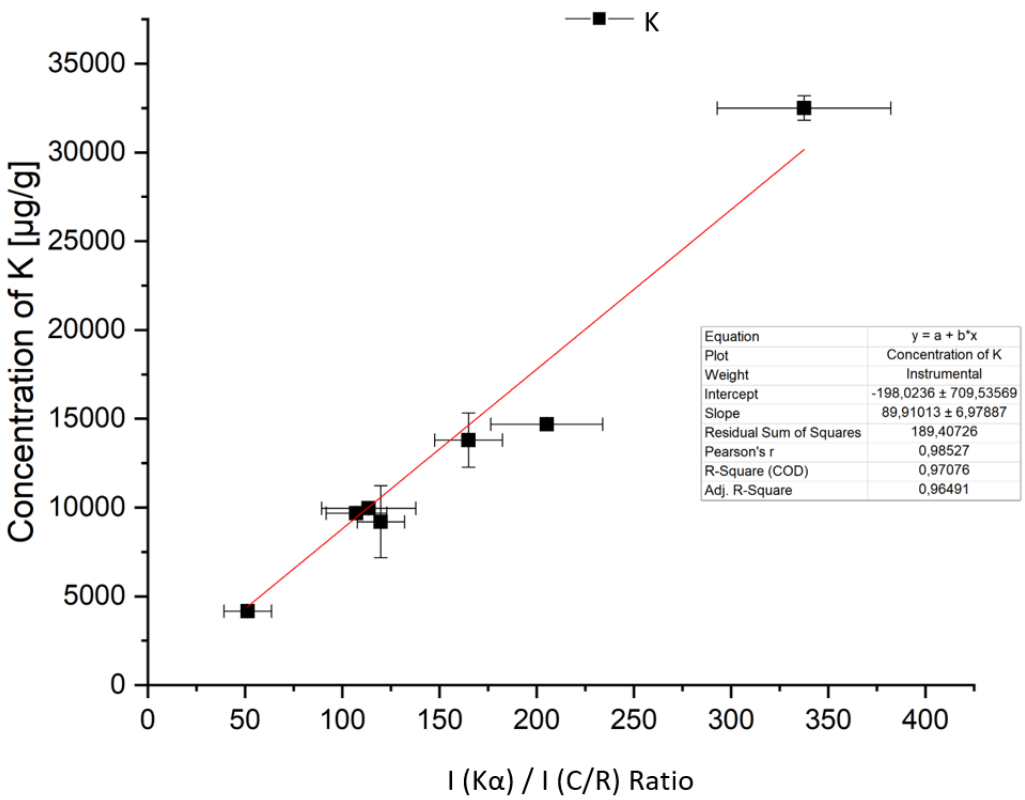

Figure 5.9: Concentration in the CRM as a function of the I(Kα) / I(C/R) ratio

For every interest element - K, Ca, Cl, Cu, Fe, Mn, P, S and Zn - the calibration curves and respective equations were obtained by the same methodology:

$$\text{Concentration}(K) = (89,91 \pm 6,98) \times \frac{K\alpha}{Ratio} + (-198,02 \pm 709,54) \tag{5.1}$$

$$\text{Concentration}(Ca) = (66,90 \pm 11,74) \times \frac{K\alpha}{Ratio} + (-2040,52 \pm 1346,40) \tag{5.2}$$

$$\text{Concentration}(Cl) = (214,71 \pm 3,69) \times \frac{K\alpha}{Ratio} + (127,31 \pm 190,78) \tag{5.3}$$

$$\text{Concentration}(Cu) = (5,77 \pm 1,20) \times \frac{K\alpha}{Ratio} + (-22,32 \pm 6,41) \tag{5.4}$$

$$\text{Concentration}(Fe) = (15,61 \pm 1,46) \times \frac{K\alpha}{Ratio} + (-81,05 \pm 13,78) \tag{5.5}$$

$$\text{Concentration}(Mn) = (6,98 \pm 0,68) \times \frac{K\alpha}{Ratio} + (8,48 \pm 1,48) \tag{5.6}$$

$$\text{Concentration}(P) = (1073,13 \pm 26,02) \times \frac{K\alpha}{Ratio} + (-981,47 \pm 220,14) \tag{5.7}$$

$$\text{Concentration}(S) = (378,03 \pm 0,25) \times \frac{K\alpha}{Ratio} + (285,75 \pm 3,49) \tag{5.8}$$

$$\text{Concentration}(Zn) = (5,30 \pm 0,50) \times \frac{K\alpha}{Ratio} + (7,12 \pm 5,19) \tag{5.9}$$

Two CRMs, NIST SRM 1566b Oyster Tissue and NIST GBW 07605 Tea, were used in order to evaluate the method's accuracy and the validity of the curves. The obtained concentrations and the relative deviation from the certified value are shown in table 5.5, for Phosphorus, as an example.

As can be observed, for both CRMs, the values obtained for the concentration of K with the calibration curve are close to the NIST certified value, presenting an accuracy of 97% for the Oyster Tissue and 71% for the Tea Leaves. The validation results for the other interest elements can be observed in the following tables:

Table 5.5: Comparison of the NIST certified P concentration and the obtained using the calibration curves for NIST SRM 1566b Oyster Tissue and NIST GBW 07605 Tea (in μg/g).

Concentration (P)	Obtained Value	NIST Value	Percent Error (%)
SRM 1566b Oyster Tissue	8000 ± 1140	-	-
GBW 07605 Tea	2700 ± 230	2840 ± 200	5

Table 5.6: Comparison of the NIST certified S concentration and the obtained using the calibration curves for NIST SRM 1566b Oyster Tissue and NIST GBW 07605 Tea (in μg/g).

Concentration (S)	Obtained Value	NIST Value	Percent Error (%)
SRM 1566b Oyster Tissue	5610 ± 1100	6890 ± 140	19
GBW 07605 Tea	2300 ± 190	2450 ± 441	6

Table 5.7: Comparison of the NIST certified Cl concentration and the obtained using the calibration curves for NIST SRM 1566b Oyster Tissue and NIST GBW 07605 Tea (in μg/g).

Concentration (Cl)	Obtained Value	NIST Value	Percent Error (%)
SRM 1566b Oyster Tissue	5810 ± 860	5140 ± 100	13
GBW 07605 Tea	-	-	-

Table 5.8: Comparison of the NIST certified K concentration and the obtained using the calibration curves for NIST SRM 1566b Oyster Tissue and NIST GBW 07605 Tea (in μg/g).

Concentration (K)	Obtained Value	NIST Value	Percent Error (%)
SRM 1566b Oyster Tissue	6720 ± 1440	6520 ± 90	3
GBW 07605 Tea	21470 ± 2500	16600 ± 2490	29

Table 5.9: Comparison of the NIST certified Ca concentration and the obtained using the calibration curves for NIST SRM 1566b Oyster Tissue and NIST GBW 07605 Tea (in μg/g).

Concentration (Ca)	Obtained Value	NIST Value	Percent Error (%)
SRM 1566b Oyster Tissue	-848 ± 1360	838 ± 168	
GBW 07605 Tea	1656 ± 1380	4300 ± 817	61

Table 5.10: Comparison of the NIST certified Mn concentration and the obtained using the calibration curves for NIST SRM 1566b Oyster Tissue and NIST GBW 07605 Tea (in μg/g).

Concentration (Mn)	Obtained Value	NIST Value	Percent Error (%)
SRM 1566b Oyster Tissue	17.2 ± 21.1	18.5 ± 0.2	7
GBW 07605 Tea	975 ± 98	1240 ± 149	21

Table 5.11: Comparison of the NIST certified Fe concentration and the obtained using the calibration curves for NIST SRM 1566b Oyster Tissue and NIST GBW 07605 Tea (in μg/g).

Concentration (Fe)	Obtained Value	NIST Value	Percent Error (%)
SRM 1566b Oyster Tissue	353 ± 80	206 ± 7	71
GBW 07605 Tea	273 ± 30	264 ± 32	3

Table 5.12: Comparison of the NIST certified Cu concentration and the obtained using the calibration curves for NIST SRM 1566b Oyster Tissue and NIST GBW 07605 Tea (in μg/g).

Concentration (Cu)	Obtained Value	NIST Value	Percent Error (%)
SRM 1566b Oyster Tissue	53 ± 15	72 ± 2	26
GBW 07605 Tea	-	-	-

Table 5.13: Comparison of the NIST certified Zn concentration and the obtained using the calibration curves for NIST SRM 1566b Oyster Tissue and NIST GBW 07605 Tea (in μg/g).

Concentration (Zn)	Obtained Value	NIST Value	Percent Error (%)
SRM 1566b Oyster Tissue	1450 ± 250	1424 ± 90	2
GBW 07605 Tea	18 ± 13	26 ± 4	31

Observing the validation results for the two chosen CRM, only the Ca concentration shows worst results, agreeing with its calibration curve, that has an R-Square value of only 0.90. For the other 8 elements, the validation present what it was expected. This could mean that the correction performed by subtracting the Kb value of K from the Ka value of Ca was not enough. This could be due to the use of the tabulated intensity ratios for infinitely thin samples, not the case for our real samples. Other reason for this curve not to work is that matrix effects (the secondary ionization of K by Ca) occur in greater extent in some CRMs than in others (due to the very different compositions of these elements), leading to a inaccurate calibration curve. Further work must be done to optimize this quantification approach, however, our main goal in this work is to study the behaviour of P, Ca and K.

5.2.2.4 Tissues' Elemental Concentration

The main goal of this master thesis is to develop a parameterization model of elemental intensity as a function of time preserved in formalin. For that, since the tissue concentrations over the time were unknown it was necessary to have calibration curves that could relate each elemental concentration with the peak intensity in the spectrum. Having achieved and validated it, as described in the previous subsection, it is possible to parameterize the elemental intensity as a function of time preserved in formalin. For that, the background removal, peaks finding and correction methodology using ROOT, Excel and OiginPro was once again used after obtaining the spectrum for all the times mentioned in 5.1 with M4 Tornado. Figure 5.10 shows an example of one of the obtained spectra from the 334 fresh sample.

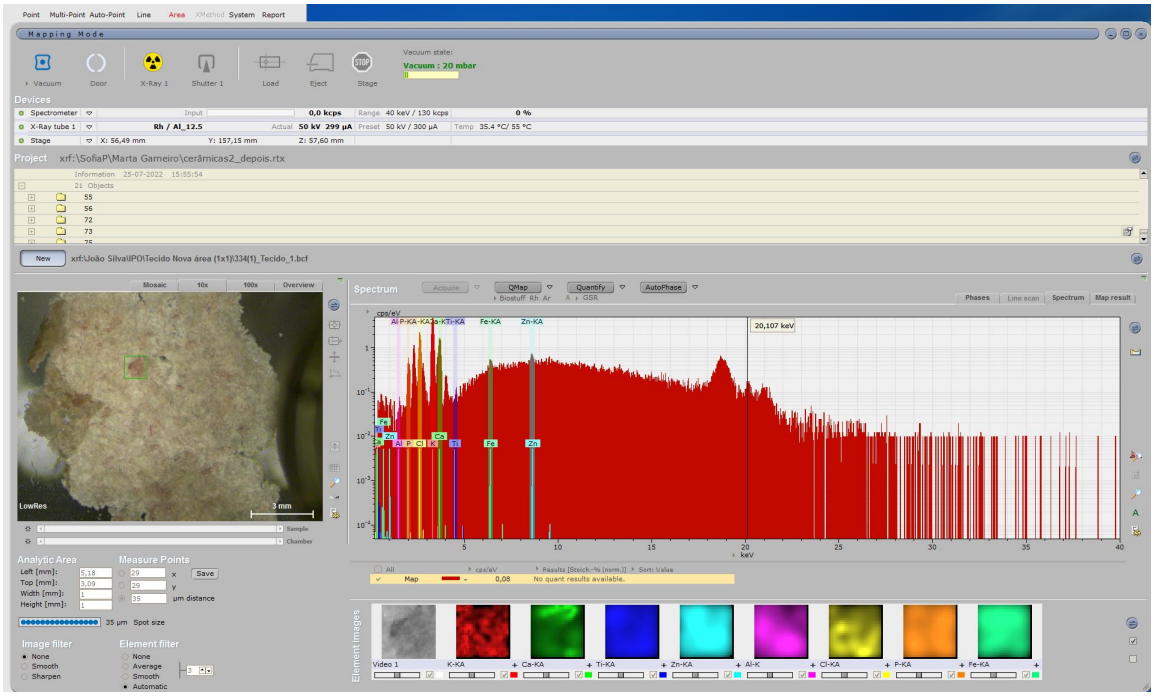

Figure 5.10: Spectra obtained with M4 Tornado software of the 334 fresh sample

With the help of the ROOT functionalities and the algorithm outputs, already described, the background was effectively removed and the identification and correction of each peak occurred as described in 5.2.2.1 and 5.2.2.2. Figure 5.11, shows the fresh sample 332, after removing the background.

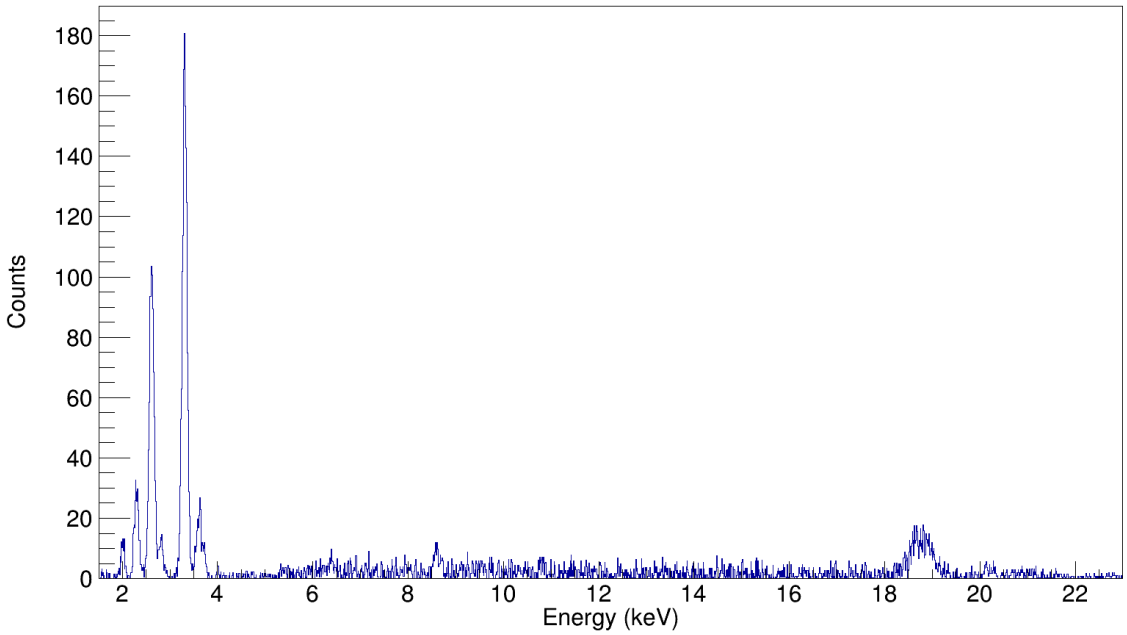

Figure 5.11: X-ray fluorescence acquired spectrum after background removal for the fresh sample 332

Thus, after replicating this process to all the fixation times of all the sets, the Kα amplitude, submitted to the mentioned corrections, was used to calculate the elemental concentration, using the elemental calibration curves, as shown in the example of table 5.12 for fresh sample 331:

		Kα Amplitude	Kβ Amplitude	Compton Amplitude
331 - Fresh Sample	_1	158,145	22,140	11,915
	_2	215,311	30,144	11,818
	_3	203,805	28,533	11,716
		Rayleigh Amplitude	Ratio (Compton/Rayleigh)	Kα / Ratio
	_1	1,516	7,859	20,124
	_2	1,637	7,220	29,822
	_3	1,471	7,965	25,588
		Mean [Kα / Ratio]	Mean Deviation	Maximum Deviation from the Mean
	_1		5,054	
	_2	25,178	4,644	5,054
	_3		0,410	
		K Concentration in [µg/g]	Uncertainty of K Concentration in [µg/g]	Final K Concentration [µg/g]
	_1			
	_2	2065,736	837,316	2065,736 ± 837,316
	_3			

Figure 5.12: 331 Fresh sample data treatment and determination of the K concentration (in μg/g).

All data related to each time interval were aggregated, that is, the results obtained from each set for each defined time were considered. So, for each time interval, I used the results of the 6 sets. By using this approach, the relative uncertainty for the concentration value rose, comparing with if each set was treated separately. This happens due to the heterogeneity between sample sets. However, by doing it, more data was used to determine each elemental concentration value as a function of a specific time, resulting in just one plot of this variation for each element, instead of 6 plots (one per set) for the respective element. Table 5.13 shows an example of the variation of K concentration for different times. It is only displayed until the 3 hours because from there on Potassium was no longer detected.

For the remaining elements, the methodology was the same, bridging with the input of the time, mean elemental concentration and its uncertainty into OriginPro, in order to plot this variation and parameterize each elemental concentration as a function of the time fixated in formalin.

After applying the calibration curves to each element, in order to determine the concentration values, some of them - Cu, Fe and Mn - were discarded, once the elements were almost undetectable for most of the times. Consequently, the analysis did not undergo alterations for the remaining elements - K, Zn, Cl, P and S.

Time (hours)	K Concentration (µg/g)	K Concentration Uncertainty (µg/g)	Mean K Concentration (µg/g)	Mean K Concentration Uncertainty (µg/g)
0	12788,305	1299,601	7486	6236
	7753,294	3084,593		
	7301,244	1239,507		
	2065,736	837,316		
	-	-		
	7520,614	1275,175		
	-	-		
0.25	659,167	715,735	2125	2089
	592,517	719,831		
	3001,686	1343,043		
	2646,622	794,659		
	3724,931	851,849		
	2951,554	3091,712		
0.5	309,004	713,532	1178	3564
	307,044	723,388		
	361,217	713,341		
	1968,420	763,842		
	1169,371	818,888		
	625,275	738,441		
1	BDL	BDL	410	925
	BDL	BDL		
	BDL	BDL		
	62,423	709,830		
	541,141	857,536		
3	BDL	BDL	BDL	BDL
	BDL	BDL		
	BDL	BDL		
	BDL	BDL		
	BDL	BDL		
	BDL	BDL		

Figure 5.13: Determination of K concentration (in μg/g) for different periods of time

The figure 5.14 synthesizes and clarifies the whole methodology explained above, by showing the major steps taken to achieve the proposed goal:

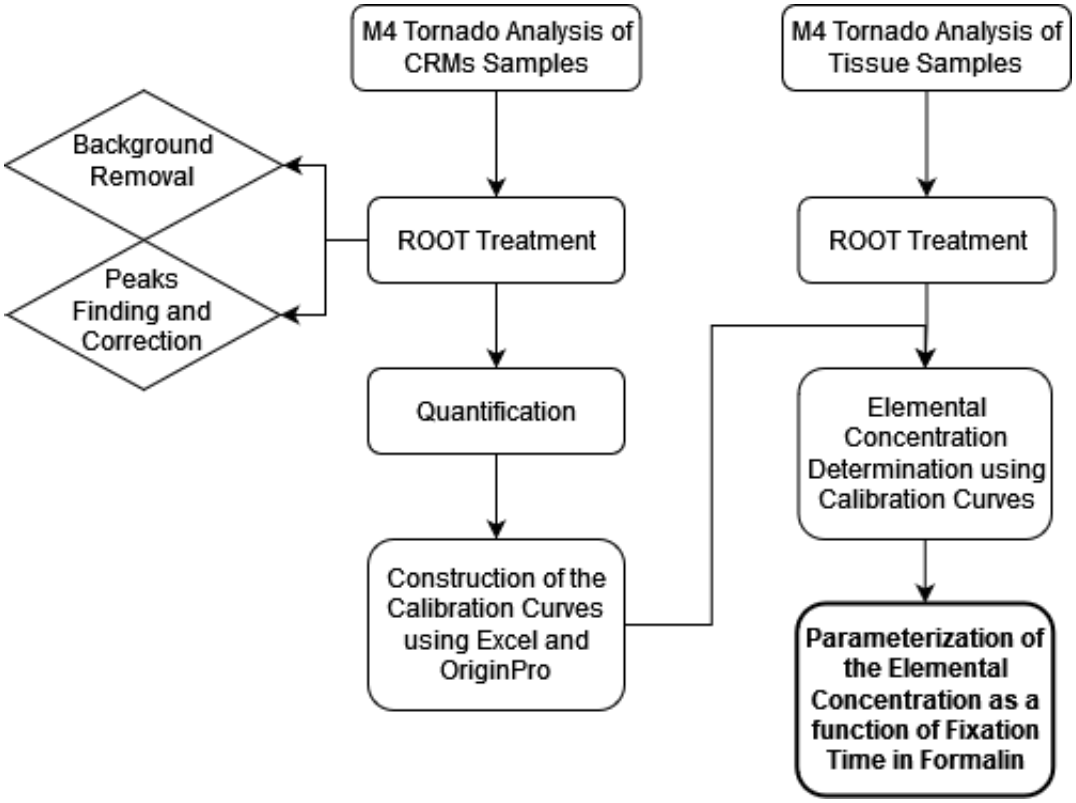

Figure 5.14: Data Treatment Synthesis

In order to study and discuss the results statistic tests were taken. First to test the normality of the data distribution, it was used the Shapiro-Wilk test. Since for some intervals, normal distribution was not followed, the non parametric test Kruskal-Wallis ANOVA was used.

Sample size (N=6) was determined according to Dell et al [39], based on the previous work of Alexandre Veiga and considering a confidence level of 95%. This sample size is enough to compare the difference of times, however, in order to obtain a robust behaviour curve with lower uncertainty, the number of tissues sampled must be higher and the tissues themselves should be more homogeneous.

6

Results and Discussion

After describing all the chosen methodology for this approach on the previous chapter, this section presents all the obtained results during this study and the respective discussion and considerations.

The preliminary results obtained in this work, referring to the influence of formalin on XRF measurements in tissue samples after two days of fixation time, are presented on chapter 4 and were the staple behind the progression of my work, showing the need to understand what variations on the elemental concentration occur on the first 48 hours of fixation time.

Since the approach to the construction of the calibration curves through CRMs was already explained on the previous chapter, and both equations and a plot example were already presented, the results on the next section will only refer to the determination of the tissues' elemental concentration

6.1 Influence of Formalin Fixation Time on the Elemental Concentration of Tissues

As mentioned on 5.2.2.3, the calibration curves were validated by two CRMs: NIST SRM 1566b Oyster Tissue and NIST GBW 07605 Tea. Thus, they were used in the determination of each tissues' elemental concentration, for the times presented on the table 5.1. For all sets' samples three spectra were obtained from various regions of the tissue as a way to reduce statistical and heterogeneity mistakes, as mentioned on the previous chapter. So, after treating all this data, with the softwares and methods already mentioned and described before, I was able to determine the tissues' elemental concentration for each time of interest.

Gathering all the sets, looking forward to have the most information to study the relation between the elemental concentration and fixation time, I was able to calculate, for each interval, the mean value for the elements' concentration. An example of this method, for K, can be observed on table 5.13.

6.1.1 Influence of Formalin Fixation Time on K Concentration

The results presented for K reflect what was expected since the preliminary phase of my master thesis, this is, a rapid decrease in concentration, eventually reaching a plateau, long before the third day.

By analysing each set response at a time, although their initial concentrations are different, the decrease rate shows a similar behavior in all of them. When joining all the sets and using its mean value for each time, the initial K concentration, meaning the concentration of K on tissues that were not formalin fixed, is 7500 ± 5400 μg/g.

According to the obtained results, after just 15 minutes of formalin fixation, the concentration of K decreased by 72% and reached its lowest value within an hour. After 3 hours, K no longer appears on the quantified samples, thus reaching and remaining on a plateau for the rest of the studied times.

Figure 6.1 shows the temporal evolution of the K concentration as well as the exponential decay fit used to parameterize it:

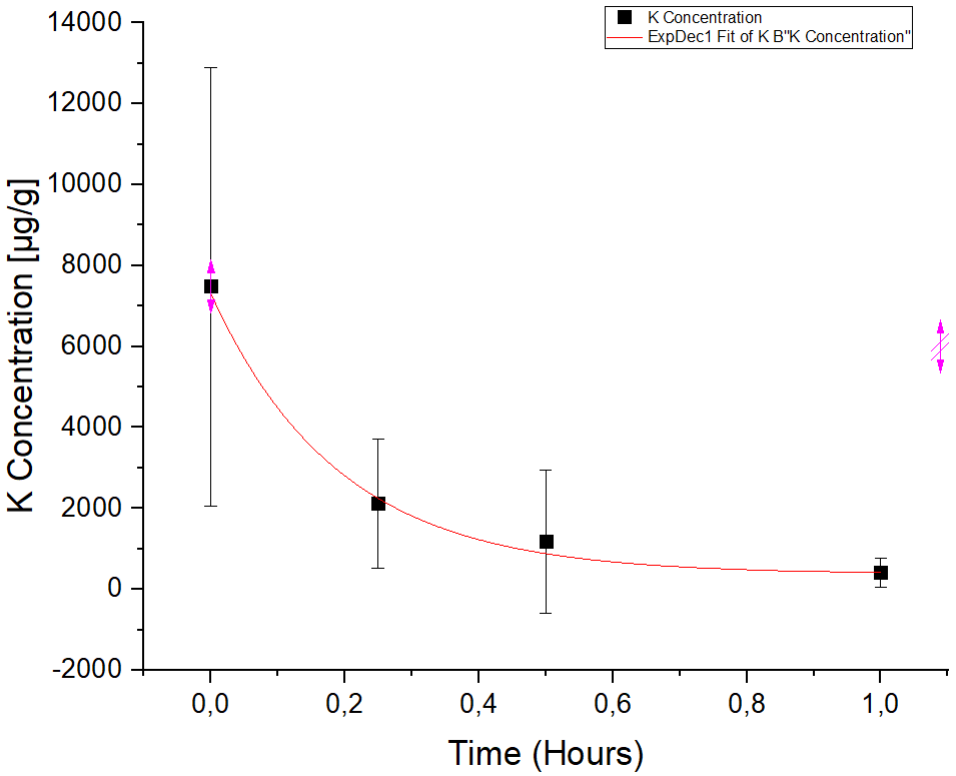

Figure 6.1: Plot of the variation of the K concentration [μg/g] in IPO tissues as a function of fixation time in formalin.

The exponential decay fit presents a R-Square value of 0.98795, and the resulting equation that parameterizes the concentration of K as a function of fixation time in

formalin is shown in the equation 6.1:

$$\text{Concentration } (K) = 6935 \pm 983 \times e^{\left(\frac{-\text{Time in Formalin}}{0.190 \pm 0.030}\right)} + 380 \pm 75 \tag{6.1}$$

Statistic test Shapiro-Wilk was performed, firstly, in order to see if the data followed a normal distribution. Since, in some time intervals did not, as shown in the figure 6.2, the non-parametric test Kruskal-Wallis ANOVA was used to compare each interval between themselves.

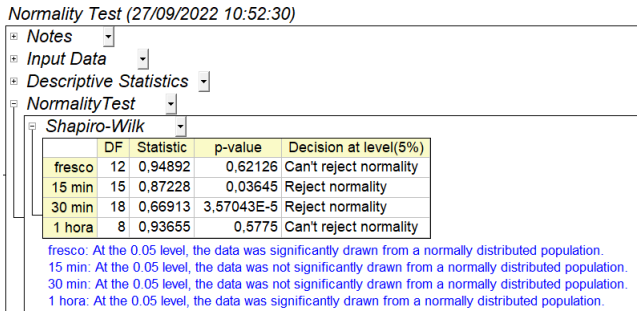
Normality Test (27/09/2022 10:52:30)
Notes
Input Data
Descriptive Statistics
NormalityTest
Shapiro-Wilk

	DF	Statistic	p-value	Decision at level(5%)
fresco	12	0,94892	0,62126	Can't reject normality
15 min	15	0,87228	0,03645	Reject normality
30 min	18	0,66913	3,57043E-5	Reject normality
1 hora	8	0,93655	0,5775	Can't reject normality

fresco: At the 0.05 level, the data was significantly drawn from a normally distributed population.
15 min: At the 0.05 level, the data was not significantly drawn from a normally distributed population.
30 min: At the 0.05 level, the data was not significantly drawn from a normally distributed population.
1 hora: At the 0.05 level, the data was significantly drawn from a normally distributed population.

Figure 6.2: Shapiro-Wilk normality test for K

Until the 3 hours range, the statistic test showed that the values were significally different. From the third hour to the next interval - 4.5 hours -, and so on, the statistic test revealed that the values were not significantly different, as shown in figure 6.3 proven that the K concentration has reached its plateau and stabilized.

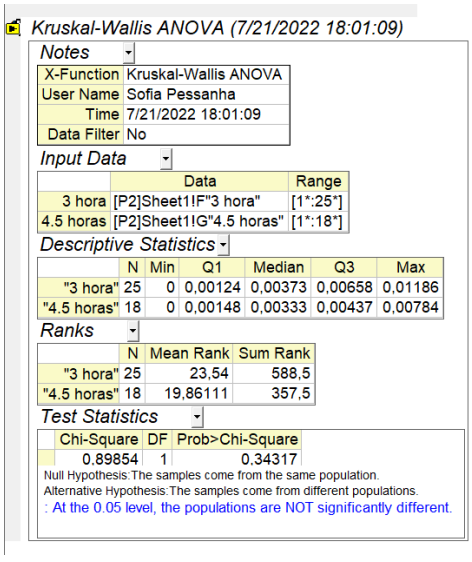
Kruskal-Wallis ANOVA (7/21/2022 18:01:09)
Notes

X-Function	Kruskal-Wallis ANOVA
User Name	Sofia Pessanha
Time	7/21/2022 18:01:09
Data Filter	No

Input Data

	Data	Range
3 hora	[P2]Sheet1!F"3 hora"	[1*:25*]
4.5 horas	[P2]Sheet1!G"4.5 horas"	[1*:18*]

Descriptive Statistics

	N	Min	Q1	Median	Q3	Max
"3 hora"	25	0	0,00124	0,00373	0,00658	0,01186
"4.5 horas"	18	0	0,00148	0,00333	0,00437	0,00784

Ranks

	N	Mean Rank	Sum Rank
"3 hora"	25	23,54	588,5
"4.5 horas"	18	19,86111	357,5

Test Statistics

Chi-Square	DF	Prob>Chi-Square
0.89854	1	0.34317

Null Hypothesis:The samples come from the same population.
Alternative Hypothesis:The samples come from different populations.
: At the 0.05 level, the populations are NOT significantly different.

Figure 6.3: Kruskal-Wallis ANOVA test for K

6.1.2 Influence of Formalin Fixation Time on Cl Concentration

According to the obtained results, Cl presents a similar behaviour to K. Beginning with an almost identical initial concentration to K, in the first 15 minutes there is a sudden decrease of 74 % in its concentration. In the following 15 minutes, it is also spotted a decrease in its value, although much more subtle than in the first 15 minutes. Even though, a value for the Cl concentration was found, before staying bellow the detection limit, at the 3 hours range, it appears to be in the plateau since the first passed hour.

Ón the figure 6.4, it is shown the temporal evolution of the Cl concentration as well as the exponential decay fit used to parameterize it:

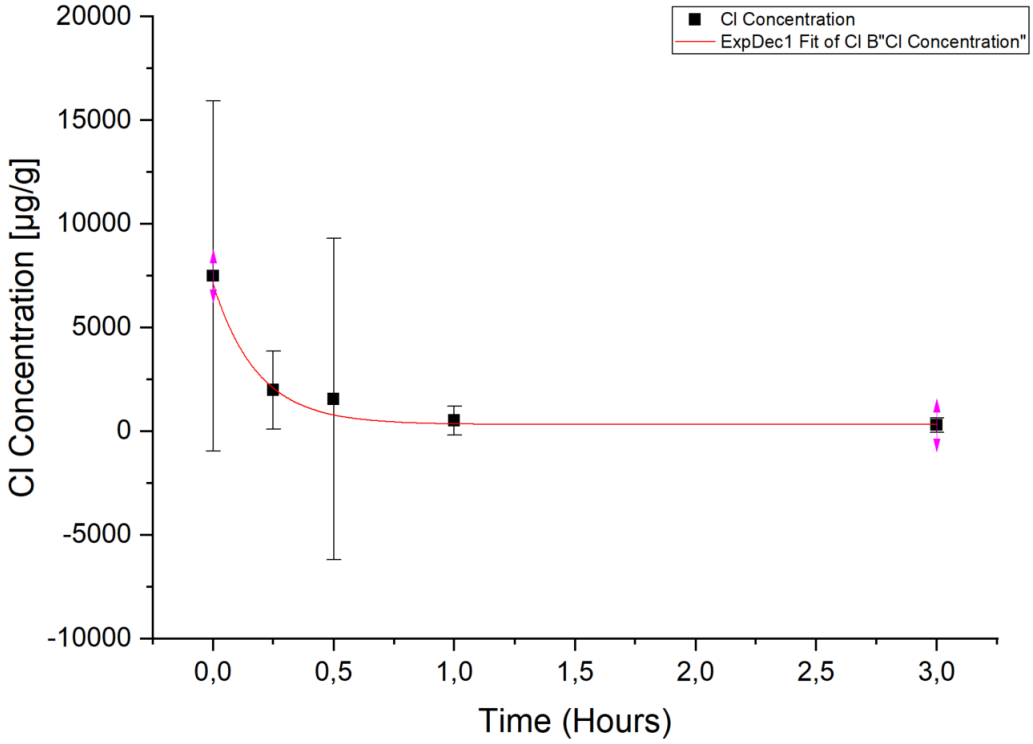

Figure 6.4: Plot of the variation of the Cl concentration [μg/g] in IPO tissues as a function of fixation time in formalin.

The characteristic R-Square value for the exponential decay fit is 0.94942, and the resulting equation that parameterizes the concentration of Cl as a function of formalin fixation time is presented on equation 6.2

$$\text{Concentration } (Cl) = 6775 \pm 1650 \times e^{\left(\frac{-\text{Time in Formalin}}{0.185 \pm 0.04}\right)} + 330 \pm 65 \tag{6.2}$$

As per K, statistic test Shapiro-Wilk was performed too, firstly, in order to see if the data followed a normal distribution, as shown in figure 6.5. Since, in some time intervals did not, the non-parametric test Kruskal-Wallis ANOVA was used to compare each interval between themselves.

Normality Test (27/09/2022 11:22:46)

Notes

Input Data

Descriptive Statistics

NormalityTest

Shapiro-Wilk

	DF	Statistic	p-value	Decision at level(5%)
fresco	12	0,92642	0,34373	Can't reject normality
15 min	15	0,93689	0,34489	Can't reject normality
30 min	14	0,49319	5,24057E-6	Reject normality
1 hora	11	0,95046	0,64981	Can't reject normality
48 horas	6	0,935	0,61925	Can't reject normality

fresco: At the 0.05 level, the data was significantly drawn from a normally distributed population.
15 min: At the 0.05 level, the data was significantly drawn from a normally distributed population.
30 min: At the 0.05 level, the data was not significantly drawn from a normally distributed population.
1 hora: At the 0.05 level, the data was significantly drawn from a normally distributed population.
48 horas: At the 0.05 level, the data was significantly drawn from a normally distributed population.

Figure 6.5: Shapiro-Wilk normality test for Cl

As mentioned before, between the 15 minutes and the 30 minutes there is a subtle decrease in the Cl concentration mean value. Analysing the obtained output of the Kruskal-Wallis ANOVA test for that time range, the Cl concentration values are not significantly different. From there to the 1 hour, the test shows that the populations are again significantly different. Comparing the 1 hour and 3 hours results the statistic test confirms that the plateau has been reached, outputting that the values are not significantly different, as shown in fig 6.6:

Kruskal-Wallis ANOVA (27/09/2022 15:49:57)

Notes

X-Function	Kruskal-Wallis ANOVA
User Name	Joaot
Time	27/09/2022 15:49:57
Data Filter	No

Input Data

	Data	Range
Group Range	[P2]Sheet1!E"1 hora"	[1*:23*]
Data Range	[P2]Sheet1!F"3 hora"	[1*:25*]

Descriptive Statistics

	N	Min	Q1	Median	Q3	Max
"1 hora"	11	231,67086	356,29343	515,1617	750,67973	910,60164
"3 hora"	1	0	0	0	0	0

Ranks

	N	Mean Rank	Sum Rank
"1 hora"	11	7	77
"3 hora"	1	1	1

Test Statistics

	Chi-Square	DF	Prob>Chi-Square
	2,53846	1	0,1111

Null Hypothesis:The samples come from the same population.
Alternative Hypothesis:The samples come from different populations.
: At the 0.05 level, the populations are NOT significantly different.

Figure 6.6: Kruskal-Wallis ANOVA test for Cl

6.1.3 Influence of Formalin Fixation Time on Zn Concentration

The results presented for Zn shows that the elemental concentration remains almost the same, over the first 48 hours. In the first 30 minutes, a 60% increase is verified. From there, the Zn concentration comes back to the initial value and remains almost constant.

As it happens with K, for the Zn case each set, although having different initial concentrations, shows a similar behavior in all of them. When joining all the sets and using

its mean value for each time, the initial Zn concentration, meaning the concentration of Zn on tissues that were not formalin fixed, is 24 ± 21 μg/g, and its concentration, after 48 hours is 20 ± 21 μg/g.

According to the obtained results, although although there are small fluctuations the concentration of Zn remains practically constant.

Figure 6.7 shows the temporal evolution of the Zn concentration as well as the exponential decay fit used to parameterize it:

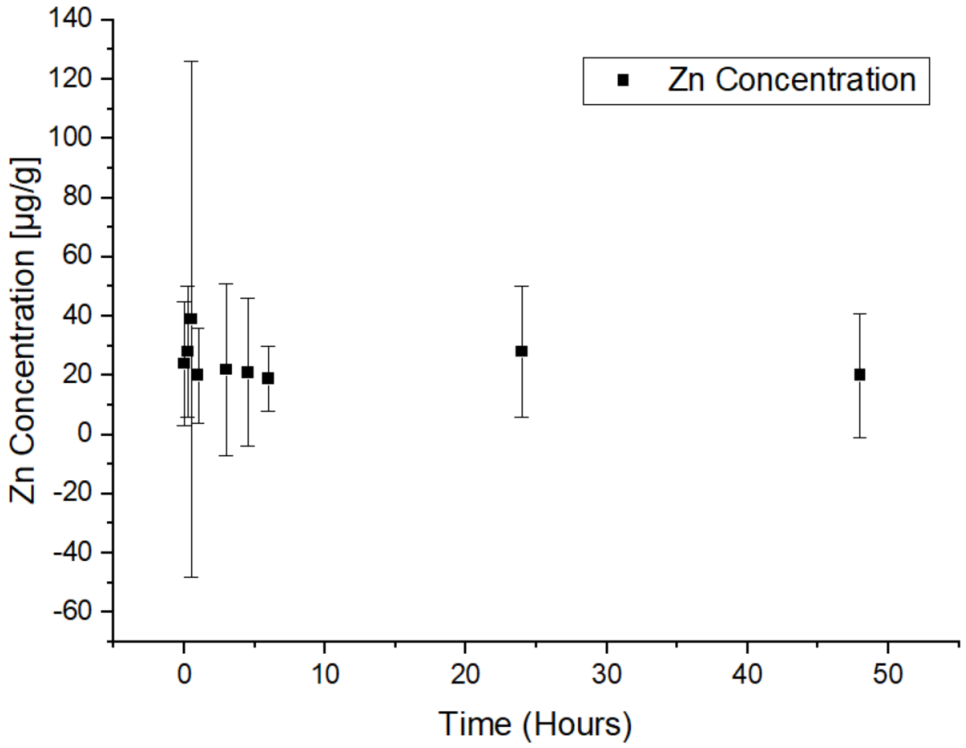

Figure 6.7: Plot of the variation of the Zn concentration [μg/g] in IPO tissues as a function of fixation time in formalin.

The previously mentioned statistic tests were performed, firstly, in order to see if the data followed a normal distribution, as shown in figure 6.8. Since, in some time intervals did not, as shown in the figure 6.8, the non-parametric test Kruskal-Wallis ANOVA was used to compare each interval between themselves.

Normality Test (27/09/2022 16:12:47)

Notes

Input Data

Descriptive Statistics

NormalityTest

Shapiro-Wilk

	DF	Statistic	p-value	Decision at level(5%)
fresco	11	0,88575	0,123	Can't reject normality
15 min	15	0,96636	0,80099	Can't reject normality
30 min	18	0,68118	4,86429E-5	Reject normality
1 hora	12	0,96701	0,87714	Can't reject normality
3 hora	15	0,86931	0,03296	Reject normality
4.5 horas	12	0,9389	0,48389	Can't reject normality
6 horas	10	0,91012	0,28185	Can't reject normality
24 horas	15	0,96366	0,75569	Can't reject normality
48 horas	18	0,89922	0,05569	Can't reject normality

fresco: At the 0.05 level, the data was significantly drawn from a normally distributed population.
15 min: At the 0.05 level, the data was significantly drawn from a normally distributed population.
30 min: At the 0.05 level, the data was not significantly drawn from a normally distributed population.
1 hora: At the 0.05 level, the data was significantly drawn from a normally distributed population.
3 hora: At the 0.05 level, the data was not significantly drawn from a normally distributed population.
4.5 horas: At the 0.05 level, the data was significantly drawn from a normally distributed population.
6 horas: At the 0.05 level, the data was significantly drawn from a normally distributed population.
24 horas: At the 0.05 level, the data was significantly drawn from a normally distributed population.
48 horas: At the 0.05 level, the data was significantly drawn from a normally distributed population.

Figure 6.8: Shapiro-Wilk normality test for Zn

By analysing the obtained output of the Kruskal-Wallis ANOVA test, the Zn concentration values are significantly different until the 1 hour range. From there on, the test shows that the populations are not significantly different, as shown in figure 6.9:

Kruskal-Wallis ANOVA (27/09/2022 16:16:06)

Notes

X-Function	Kruskal-Wallis ANOVA
User Name	Joaot
Time	27/09/2022 16:16:06
Data Filter	No

Input Data

	Data	Range
Group Range	[P2]Sheet1!E"1 hora"	[1":23"]
Data Range	[P2]Sheet1!F"3 hora"	[1":25"]

Descriptive Statistics

	N	Min	Q1	Median	Q3	Max
"1 hora"	12	10,70722	17,15229	19,18152	24,39586	33,61758
"3 hora"	15	11,4144	14,21535	16,72251	26,16495	42,80824

Ranks

	N	Mean Rank	Sum Rank
"1 hora"	12	14,91667	179
"3 hora"	15	13,26667	199

Test Statistics

Chi-Square	DF	Prob>Chi-Square
0,2881	1	0,59144

Null Hypothesis:The samples come from the same population.
Alternative Hypothesis:The samples come from different populations.
: At the 0.05 level, the populations are NOT significantly different.

Figure 6.9: Kruskal-Wallis ANOVA test for Zn

6.1.4 Influence of Formalin Fixation Time on P Concentration

As in the case of Zn, P is detected for all the time intervals, never becoming bellow the detection limit. By analysing the obtained results, P remains on a cycle. When formalin has contact with the tissues, it is detected an increase in P concentration in the first 30 minutes. From there to the1 hour interval, it is detected a decrease followed by another increase. Remains on this cycle until the 48 hours, as shown in figure 6.10:

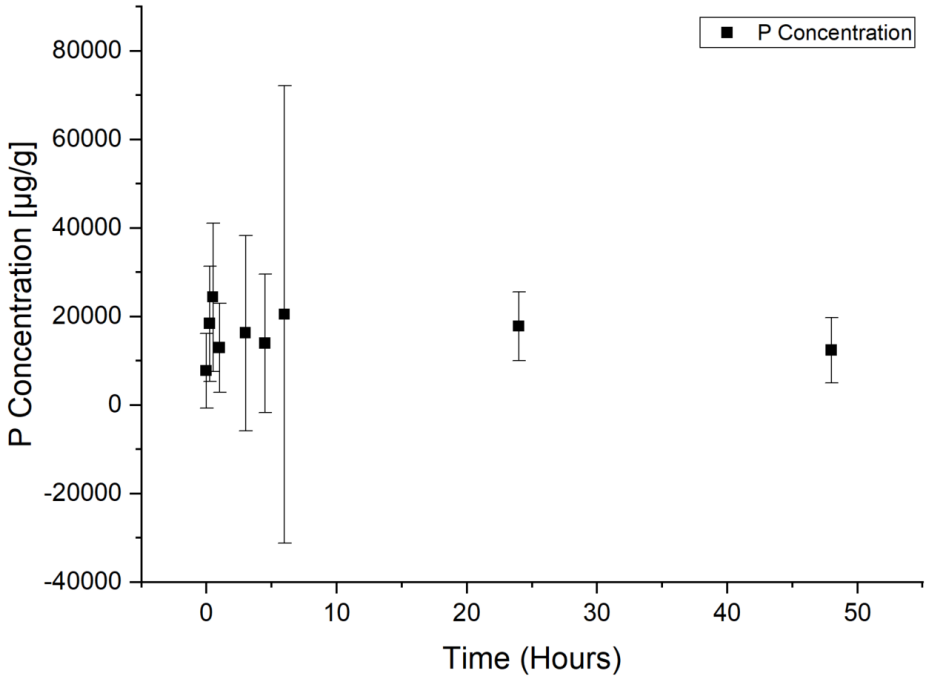

Figure 6.10: Plot of the variation of the P concentration [μg/g] in IPO tissues as a function of fixation time in formalin.

By performing the chosen, already described, statistic testes, the values are significantly different for the time intervals: 0 hours to 15 minutes, 30 minutes to 1 hour, 6 hours to 24 hours and 24 hours to 48 hours.

6.1.5 Influence of Formalin Fixation Time on S Concentration

Sulfur is another element that has its concentration affected by formalin fixation time but never decreases bellow the detection limit. The initial concentration of this element on the tissue, before contacting with formalin, is 6100 ± 5150 μg/g remaining almost constant, or just with subtle variations, in almost every time interval, as shown in figure 6.11

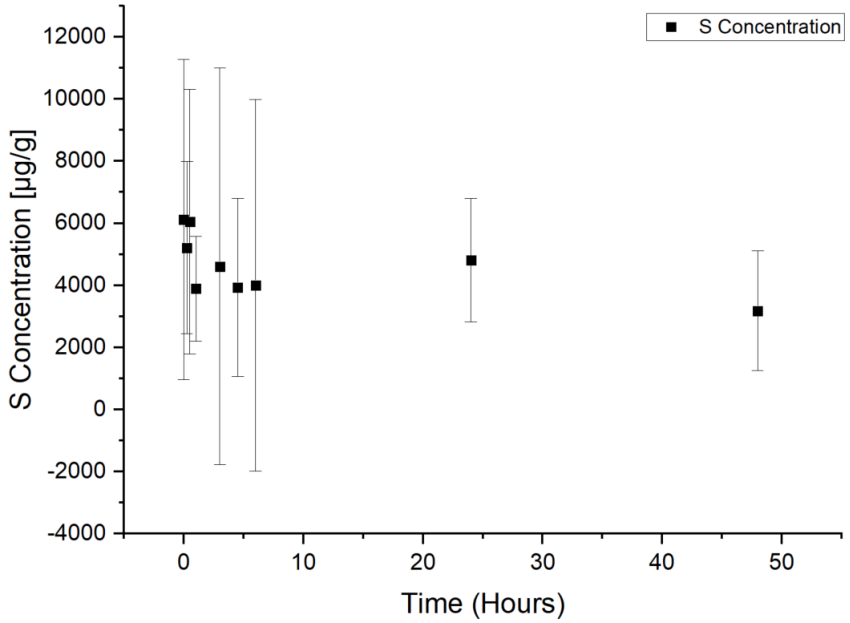

Figure 6.11: Plot of the variation of the S concentration [μg/g] in IPO tissues as a function of fixation time in formalin.

By performing the statistical tests, only from the 6 to 24 hours and 24 to 48 hours interval the outputs show that the values are significantly different.

6.1.6 Accuracy of the Results

After analyzing all the obtained results and parameterizing the variation of K and Cl concentration as a function of time, the last step was to test the parameterizations. To do that, 2 new samples were used - one from the 330 set and another from the 334 - and 2 different time intervals were chosen - 10 and 40 minutes. The sample from the set 334 was formalin fixated for 10 minutes and the sample from the set 330 for 40 minutes.

To validate the equations 6.1 and 6.2, the new samples were submitted to the same methodology and analyzed with the same tools. After submitting the samples to all the data treatment described in the previous chapter, the obtained results for the concentration of K and Cl by the methodology used in this work and by the equations presented in this chapter, are shown in the table 6.1 and 6.2:

Table 6.1: Comparing the obtained values of K concentration

Time (min)	K Concentration (μg/g)	K Concentration (μg/g) using the Equation
10	1400 ± 820	3260 ± 470
40	130 ± 710	590 ± 120

Analysing the K results, even considering the associated uncertainties, the obtained

value, using the equation 6.1, is greater than the calculated value using the calibration curves' methodology, showing that improvements can be made in the methodology, in order to have a parameterization for K that presents a higher accuracy and less deviation.

Table 6.2: Comparing the obtained values of Cl concentration

Time (min)	Cl Concentration (μg/g)	Cl Concentration (μg/g) using the Equation
10	2050 ± 590	3080 ± 750
40	490 ± 190	510 ± 140

On the other hand, considering the associated uncertainties, the obtained values for Cl with the equation 6.2 are closer to the obtained value with calibration curves' methodology. For the time interval of 40 minutes, the obtained values can be considered the same, proving that although the methodology could suffer some improvements in order to get an higher accuracy, the equation does a really good parameterization of the variation of Cl concentration as a function of formalin fixation time.

7

Conclusions

The main objective of this work was to study and parameterize the influence of formalin fixation time on the elemental composition of human tissues. The several methods chosen to achieve this goal were proven innovating and promising in the context of investigating the influence of formalin on trace elements' potential use as biomarkers for carcinogenesis.

During this work, there were some difficulties that need further attention in the future since the samples were smaller and more morphologically different, within themselves, than what it was requested. Besides that, some errors should be taken into account when analysing the results, such has time related errors. When preparing the samples to formalin fixate them, there are small time discrepencies between the first formalin fixated set sample and the last. This time difference may not matter when the time interval studied is 24 hours or 48 hours, but it is relevant when studying the 15 minutes interval. Although the time associatead errors and the samples' heterogeneity, the obtained results showed good accuracy, corroborating the expected behaviour. The usage of ROOT allowed to correct and minimize errors, with background removal and peaks identifying. Besides ROOT, the excel treatment and correction - Compton-to-Rayleigh ratio and the overlapping of characteristic lines of elements - also contributed to a higher accuracy of the method.

The validation showed that this work's results can be used, to possibly go back to the FFPE samples and trace elements, like K and Cl, that were no longer present due to formalin fixation time. In order to make this model more robust and decrease uncertainty in the quantification, a higher number of samples must be used, so this is a work in progress. K and Cl are two fundamental trace elements in human body. They are involved on many biochemical processes and are the staple on the study and characterization of carcinogenesis. So, understanding their behaviour on formalin is needed, since formalin is one of the most used methods of conservation of tissues in clinics, laboratories and hospitals.

7.1 Future Work

As mentioned in previous chapters, one of the obstacles faced in this master thesis was the heterogeneity of the tissue samples. Although the used tissue was always muscle, each set had morphology and mass differences within it and between each other sets. This affects the interaction with the formalin. The formalin used in the fixation of the tissues, in the defined timeline, was tried to analyzed and quantify, but since the contact area is so small, and so different between samples, poor results were presented. Having larger portions of tissue and more homogeneous could solve this problem and enable the analysis of formalin on the first 48 hours to complement the tissues' analysis and quantification. It would also be important to to compare this study with another using complementary techniques, that, for example, could analyze Z<13 elements, such as PIGE. By analyzing Z<13 elements, it would be possible to quantify sodium and relate the obtained results with a biochemical process that could explain it.

Bibliography

[1] M. Yaman. "Comprehensive comparison of trace metal concentrations in cancerous and non-cancerous human tissues". In: *Current medicinal chemistry* 13.21 (2006), pp. 2513–2525 (cit. on pp. 1, 16).

[2] *"World Health Organization Website - Health Topics - Cancer"*. Accessed September 4, 2022. URL: https://www.who.int/news-room/fact-sheets/detail/cancer (cit. on p. 1).

[3] S. A. N. Silvera and T. E. Rohan. "Trace elements and cancer risk: a review of the epidemiologic evidence". In: *Cancer Causes & Control* 18.1 (2007), pp. 7–27 (cit. on p. 1).

[4] C. Theodorakou and M. J. Farquharson. "Human soft tissue analysis using x-ray or gamma-ray techniques". In: *Physics in Medicine and Biology* 53.11 (May 2008), R111–R149. DOI: 10.1088/0031-9155/53/11/r01. URL: https://doi.org/10.1088/0031-9155/53/11/r01 (cit. on p. 1).

[5] L. Carvalho et al. "Human tumour banks: imperative in medicine." In: *Acta Médica Portuguesa* 20.4 (2007), pp. 325–34 (cit. on p. 1).

[6] M. P. Silva et al. "Trace elements as tumor biomarkers and prognostic factors in breast cancer: a study through energy dispersive x-ray fluorescence". In: *BMC Research Notes* 5.1 (2012), pp. 1–11 (cit. on p. 1).

[7] J. Chwiej et al. "Preparation of tissue samples for X-ray fluorescence microscopy". In: *Spectrochimica Acta Part B: Atomic Spectroscopy* 60.12 (2005), pp. 1531–1537 (cit. on pp. 2, 18, 20).

[8] E. M. Johnston, E. Dao, and M. J. Farquharson. "Advances in the histopathological characterization of breast tissue using combined X-ray fluorescence and X-ray diffraction data in a multivariate analysis approach". In: *X-Ray Spectrometry* 48.5 (2019), pp. 432–437 (cit. on p. 2).

[9] P. Brouwer. *Theory of XRF*. Almelo, Netherlands: PANalytical BV, 2006 (cit. on pp. 4, 6, 7, 11–13).

[10] R. Van Grieken and A. Markowicz. *Handbook of X-ray Spectrometry*. CRC press, 2001 (cit. on p. 4).

[11] M. Haschke. *Laboratory micro-X-ray fluorescence spectroscopy*. Vol. 10. Cham: Springer International Publishing, 2014, pp. 3–13, 159–200 (cit. on pp. 5–10, 14, 26).

[12] R. Sitko and B. Zawisza. *Quantification in X-ray fluorescence spectrometry*. InTech Croatia, 2012, pp. 137–162 (cit. on pp. 13, 14).

[13] T. Magalhães et al. "Trace elements in human cancerous and healthy tissues from the same individual: A comparative study by TXRF and EDXRF". In: *Spectrochimica Acta Part B: Atomic Spectroscopy* 61.10 (2006). TXRF-2005, 11th International Conference on Total Reflection X-ray Fluorescence Spectrometry and Related Methods, pp. 1185–1193. ISSN: 0584-8547. DOI: https://doi.org/10.1016/j.sab.2006.06.002. URL: https://www.sciencedirect.com/science/article/pii/S0584854706001716 (cit. on p. 16).

[14] A. Ensina et al. "Analysis of human tissues using Energy Dispersive X Ray Fluorescence–Dark matrix determination for the application to cancer research". In: *Journal of Trace Elements in Medicine and Biology* 68 (2021), p. 126837 (cit. on pp. 16, 17).

[15] U. Majewska et al. "Some aspects of statistical distribution of trace element concentrations in biomedical samples". In: *Nuclear Instruments and Methods in Physics Research Section B: Beam Interactions with Materials and Atoms* 150.1-4 (1999), pp. 254–259 (cit. on p. 16).

[16] A. Kubala-Kukuś et al. "Log-stable concentration distributions of trace elements in biomedical samples". In: *Spectrochimica Acta Part B: Atomic Spectroscopy* 59.10-11 (2004), pp. 1711–1716 (cit. on p. 16).

[17] J. Machado et al. "Accuracy improvement in XRF analysis for the quantification of elements ranging from tenths to thousands μg g- 1 in human tissues using different matrix reference materials". In: *Journal of Analytical Atomic Spectrometry* 35.12 (2020), pp. 2920–2927 (cit. on pp. 17, 28, 29, 32).

[18] I. Antcheva et al. "ROOT—A C++ framework for petabyte data storage, statistical analysis and visualization". In: *Computer Physics Communications* 180.12 (2009), pp. 2499–2512 (cit. on p. 17).

[19] M. Carvalho et al. "Trace elements in human cancerous and healthy tissues: A comparative study by EDXRF, TXRF, synchrotron radiation and PIXE". In: *Spectrochimica Acta Part B: Atomic Spectroscopy* 62.9 (2007), pp. 1004–1011 (cit. on p. 17).

[20] S. J. Mulware. "Comparative trace elemental analysis in cancerous and noncancerous human tissues using PIXE". In: *Journal of biophysics* 2013 (2013) (cit. on p. 17).

[21] K. Geraki, M. Farquharson, and D. Bradley. "Concentrations of Fe, Cu and Zn in breast tissue: a synchrotron XRF study". In: *Physics in Medicine & Biology* 47.13 (2002), p. 2327 (cit. on p. 17).

[22] M. R. Gherase and D. E. Fleming. "Probing Trace Elements in Human Tissues with Synchrotron Radiation". In: *Crystals* 10.1 (2019), p. 12 (cit. on p. 17).

[23] K. N. Devi, H. N. Sarma, and S. Kumar. "Estimation of essential and trace elements in some medicinal plants by PIXE and PIGE techniques". In: *Nuclear Instruments and Methods in Physics Research Section B: Beam Interactions with Materials and Atoms* 266.8 (2008). Ion Beam Analysis, pp. 1605–1610. ISSN: 0168-583X. DOI: https://doi.org/10.1016/j.nimb.2007.12.004. URL: https://www.sciencedirect.com/science/article/pii/S0168583X07017661 (cit. on p. 17).

[24] T. Paunesku et al. "X-ray fluorescence microscopy for investigation of archival tissues". In: *Health physics* 103.2 (2012), p. 181 (cit. on p. 18).

[25] A. Veiga. "Influence of Paraffin Embedding in the Analysis of Human Biopsed Soft Tissue". MA thesis. FCT-NOVA, 2021 (cit. on pp. 18, 20–22).

[26] D. Braga. "Analysis of Trace Elements in Human Soft Tissues From Cancerous Patients Using X-Ray Fluorescence". MA thesis. FCT-NOVA, 2021 (cit. on p. 20).

[27] S. Pessanha et al. "A simple and sustainable portable triaxial energy dispersive X-ray fluorescence method for in situ multielemental analysis of mining water samples". In: *Spectrochimica Acta Part B: Atomic Spectroscopy* 164 (2020), p. 105762 (cit. on pp. 20, 21).

[28] M. Manso et al. "Unveiling the Third Secret of Fátima: μ-XRF quantitative characterization and 2D elemental mapping". In: *Spectrochimica Acta Part B: Atomic Spectroscopy* 130 (2017), pp. 35–38 (cit. on p. 22).

[29] M. Manso, S. Pessanha, and M. Carvalho. "Artificial aging processes in modern papers: X-ray spectrometry studies". In: *Spectrochimica Acta Part B: Atomic Spectroscopy* 61.8 (2006), pp. 922–928 (cit. on p. 22).

[30] M. Mazuritskiy et al. "On the Surface Structure of Microchannel Plates and the Excitation of X-Ray Fluorescence in Hollow Microcapillaries". In: *Journal of Surface Investigation: X-ray, Synchrotron and Neutron Techniques* 13.3 (2019), pp. 499–507 (cit. on p. 26).

[31] *"Bruker - M4 Tornado"*. Accessed September 7, 2022. URL: https://www.bruker.com/en/products-and-solutions/elemental-analyzers/micro-xrf-spectrometers/m4-tornado.html (cit. on pp. 26, 27).

[32] U. of Albany. *"Polycapillary Optics"*. Accessed September 7, 2022. URL: https://www.albany.edu/x-ray-optics/polycapillary_optics.htm (cit. on p. 27).

[33] *"CERN"*. Accessed September 17, 2022. URL: https://home.cern/ (cit. on p. 28).

[34] I. Antcheva et al. “ROOT—A C++ framework for petabyte data storage, statistical analysis and visualization”. In: *Computer Physics Communications* 182.6 (2011), pp. 1384–1385 (cit. on p. 28).

[35] M. Morháč et al. “Background elimination methods for multidimensional coincidence γ-ray spectra”. In: *Nuclear Instruments and Methods in Physics Research Section A: Accelerators, Spectrometers, Detectors and Associated Equipment* 401.1 (1997), pp. 113–132 (cit. on p. 28).

[36] *"NIST"*. Accessed September 20, 2022. URL: https://www.nist.gov/ (cit. on p. 30).

[37] *"X-ray Transition Energies Database - NIST"*. Accessed September 24, 2022. URL: https://physics.nist.gov/PhysRefData/XrayTrans/Html/search.html (cit. on p. 32).

[38] R. Cesareo. “X-ray physics: Interaction with matter, production, detection”. In: *La Rivista del Nuovo Cimento* 23.7 (2000), pp. 1–231 (cit. on p. 32).

[39] R. R. Dell RB Holleran S. “Sample size determination”. In: *ILAR Journal* 43 (2002), pp. 207–213 (cit. on p. 41).